APPLICATION OF GEOPHYSICAL METHODS TO DELINEATE FRESH WATER AND SALINE WATER ZONES IN AMIBARA IRRIGATION FARM LANDS AMIBARA, EASTERN ETHIOPIA

A Thesis

Presented to

The School of Graduate Studies

Addis Ababa University

In Partial Fulfillment of the Requirements for the Degree

Master of Science in Applied Geophysics

by

Abebayehu Zebene

June 2000

ACKNOWLEDGEMENTS

I would like to offer my deepest sense of gratitude and respect to my advisor Dr. Tigistu Haile for his dedication in supervising the fieldwork, limitless effort in reading the manuscript and giving his valuable comments. I am greatly indebted to my co-advisor Ato Taye Zewdie, EIGS, for his assistance in the interpretation.

I would like to extend my thanks to all members of the Geophysics Department of the EIGS for their kindness in sharing their computers and other facilities. My thanks also go to Ato Senay Mekuria for his devotion in giving me tutorials on computer usage during data processing.

My special thanks also to my wife Tsehay Kifle, without her daily encouragement and assistance in typing the manuscript; this work would not have been realized.

Lastly, but not the least, I would like to offer my thanks to Ato Tibebe Mengesha, Ministry of Water Resources, for his contribution during the field work at Amibara and all rounded assistance in the interpretation of results and Ato Dereje Ashine, Ambassel Pvt. ltd., for providing me his PC for preparing the material in the present form.

TABLE OF CONTENTS

LIST OF FIGURES AND TABLES

Figures Page

Table

ABSTRACT

With the aim to mapping the saline and fresh water interface and verifying the application of geophysical methods to study problems of salinity at the Amibara irrigation farm; electrical methods were applied over two parallel traverses.

The methods employed included Schlumberger sounding surveys at ten VES points on the two traverses with VES points spacing of 450 meters to 1100 meters and dipole-dipole surveys over four profiles of approximate length of 250 meters over the same two traverses. The dipole surveys were carried out with three levels expected to give depth of investigations of about 5, 7.5 and 10 meters.

The results of these field surveys are interpreted and presented in the form of geoelctricsections and pseudosections. A general geological section of the survey area is given from the interpretation of the sounding data.

The results have clearly mapped the different geologic horizons of the subsurface and delineated areas of low resistivity due to effects associated with highly saline formation fluids.

The work has verified the effectiveness of the electrical methods of prospecting in studying problems associated with salinity and shows the potential of these methods in planning current and near future farm land utilization and monitoring of current pilot desalination programes.

Surveys carried out over properly selected sample areas could minimize the cost of obtaining such information from expensive piezometric wells and soil test pits.

1. INTRODUCTION

1.1 General

Geophysics applies the principles of physics to the study of the earth. Geophysical investigations of the interior of the earth involve taking measurements at or near the earth's surface that are influenced by the internal distribution of physical properties. Analysis of these measurements can reveal how the physical properties of the earth's interior vary vertically and laterally.

There are various approaches available to gather information about the subsurface. The best is direct observation of the sediments and rocks themselves either by drilling bore- holes (these are expensive and provide information only at discrete locations) or by looking for deep valleys cut through an area of interest to the necessary depths so that all one needs to do is correlate geologic sections from one position to another. Of course, this is rarely possible to the extent that one would like. More commonly, when subsurface information is required, physical measurements are carried out on the surface to deduce subsurface geology. The value of geophysics is then its ability to acquire information about the subsurface over a substantial area in a reasonable time frame and in a cost-effective manner.

Geophysics essentially is the measurement of contrasts in the physical properties of materials beneath the surface of the earth and the attempt to deduce the nature and distribution of the materials responsible for these observations. Some of the physical properties of materials/bodies within the earth that are amenable to measurement are density, magnetic susceptibility and electrical properties of rocks like resistivity. Variations in elastic module and density for example, cause seismic waves to travel at different speeds through different materials. By timing the arrivals of these waves at surface observation points one can deduce a

great deal about the nature and distribution of subsurface bodies. Density variations in the subsurface, as another example, lead to variations in the gravitational acceleration at surface instrument stations, and variations in magnetic susceptibilities produce measurable differences in the magnetic field at observation sites. Variations in the electrical conductivities of rocks and sediments produce varying values of apparent resistivities as the distance between measuring electrodes is increased or as the positions of the electrodes is changed on the surface. These variations in the physical properties must be sufficiently large so that the instruments can measure their effects.

These contrasts in physical properties permit the geophysicist to map in detail, for example, bedrock topography that is present at depths. It is also possible to extract the form and distribution of alluvial sand and gravel deposits or to trace buried river channel and determine the distribution of contaminated waters flowing from a waste disposal site (Burger, 1992). Applications of geophysical methods to delineating saline and fresh water zones, location of saline groundwater inflow to a river and in defining causes of dry land salinity have been respectively reported by Roy and Elliott (1979), Odins et al. (1985) and Street and Engel (1987). In the present thesis, one of the Geophysical methods, electrical resistivity (Vertical Electrical Sounding and Profiling) was employed to delineate (map) the saline and fresh water zones in Amibara Irrigation farm which has been known to have a salinity problem. The electrical resistivity method was chosen for the work because such methods can not only map basement depth, but also directly detect groundwater, particularly when saline. Moreover the measurements are sensitive to variation in salinity. The vertical electrical resistivity soundings are the best means to obtain quantitative information both on water salinity and on the vertical distribution of permeable sandy layers and less permeable clayey horizons (Odins, et al. 1985, Van Overmeeren, 1989).

Since the major geologic unit in the study area is alluvial/colluvial deposit, good contrasts in electrical resistivity were expected between clayey and sandy layers, between water bearing and dry layers or the impervious bedrock, and between formations bearing fresh water and saline water

1.2 Salinity Problem

Principally, there are six processes, which may increase the salt content of water (Appelo and Postma, 1994). These are:

- evaporation and concentration/precipitation of dissolved salts
- dissolution of salts
- mixing with recent sea water
- mixing with old water (connate water from buried marine sediments)
- volcanic exhalations
- hyperfiltration

Accumulation of excess salts in the root zone resulting in a partial or complete loss of soil productivity is a worldwide phenomenon. The problems of soil salinity are most widespread in the arid and semi-arid regions. Soil salinity is also a serious problem in areas where groundwater of high salt content is used for irrigation. The most serious salinity problems are being faced in the irrigated arid and semi-arid regions of the world and it is in these regions that irrigation is essential to increase agricultural production. However, irrigation is often costly, technically complex and requires skilled management. Failure to apply efficient principles of water management may result in wastage of water through seepage, over-watering, and inadequate drainage that result in water logging and salinity problems that reduce the soil productivity, eventually leading to loss of cultivable land (FAO, 1988).

The success of an irrigation project or of particularly dry-land farming is dependent, amongst other factors, on the concentration of salts in the vicinity of plant roots. It is inevitable that salts are added to the soil by rain or irrigation water and the weathering of rocks in or on the soil may make a further contribution of soluble material. These salts must be leached from the root zone by some artificial or natural process in order that salinity shouldn't reach a harmful level (Peck, 1971).

According to Callinan and Webster (1971), problems resulting from high salinity in streams and shallow water tables arise frequently from the clearing of forests and from irrigation. Hence, evaluation of the consequences of salinity problems must commence with clear knowledge and understanding of the economic and social basis upon which the region functions.

The effects of high salinity can be lessened in areas that are already affected, and can be avoided in areas about to be developed. Salinity has significant social and economic consequences because it affects the life and health of plants, animals and human beings. In small quantities salt is essential to life, but in greater concentrations, frequently exceeded in nature, it kills animals and plants. Excess amounts are difficult to combat because of the large volumes to be removed from the water or soils.

Since saline and alkaline soils are characteristics of arid and semi arid regions, and the study area is grouped under semi-arid regions, reclamation of these soils and prevention of excess soluble salts in fertile areas under irrigation is of paramount importance. The scanty rains in the area do not penetrate the soils deeply enough for appreciable leaching. Low infiltration combined with excessive evaporation cause accumulation of soluble salts injurious to plant growth. In areas where there is a shallow water table either by transport of groundwater or excessive irrigation and poor drainage, the upward flow of ground water

results in continuing accumulation of salt in the surface soil. This is particularly so in the study area (Halcrow, 1983)

1.3 The Study Area

1.3.1 Location

Amibara Irrigation Project (AIP), at present known as Middle Awash Agricultural Development Enterprise, lies in the northern Rift valley region of Ethiopia in area close to the so called Afar Triangle. The project area is situated adjacent to the right-bank of the Awash River, and includes the settlements of Melka Sadi and Melka Warer. Access to the farm is provided by an all-weather link road, that connects with the Addis Ababa- Mille high way. The Rift escarpments rise some distance to the east and west of the site (Halcrow, 1986). The particular area chosen for the present work is located in the farm nearest to the area called Arage Camp, which is situated about 13 km NE of the farm town Melka Werer (Fig. 1) with in geographic coordinates 9° 22′ N - 9° 25′ N and 40° 11′ E - 40° 14′ E.

1.3.2 Topography

The topography of the study area reflects the recent geomorphologic history of the Middle Awash Valley, through which an extensive alluvial plain has been constructed by deposits from the Awash River. The present course of the river, which meanders extensively, is characterized by pronounced levee formations along the western boundary of the study area. In both Melka Sadi and Amibra plains (Fig. 1), the over all slope is away on both sides) from the river, generally along former flood paths of the river. Ground elevations range from approximately 745 m in the south to 725 m in the extreme north, descending gradually over a

FIGURE 1

STUDY AREA LOCATION

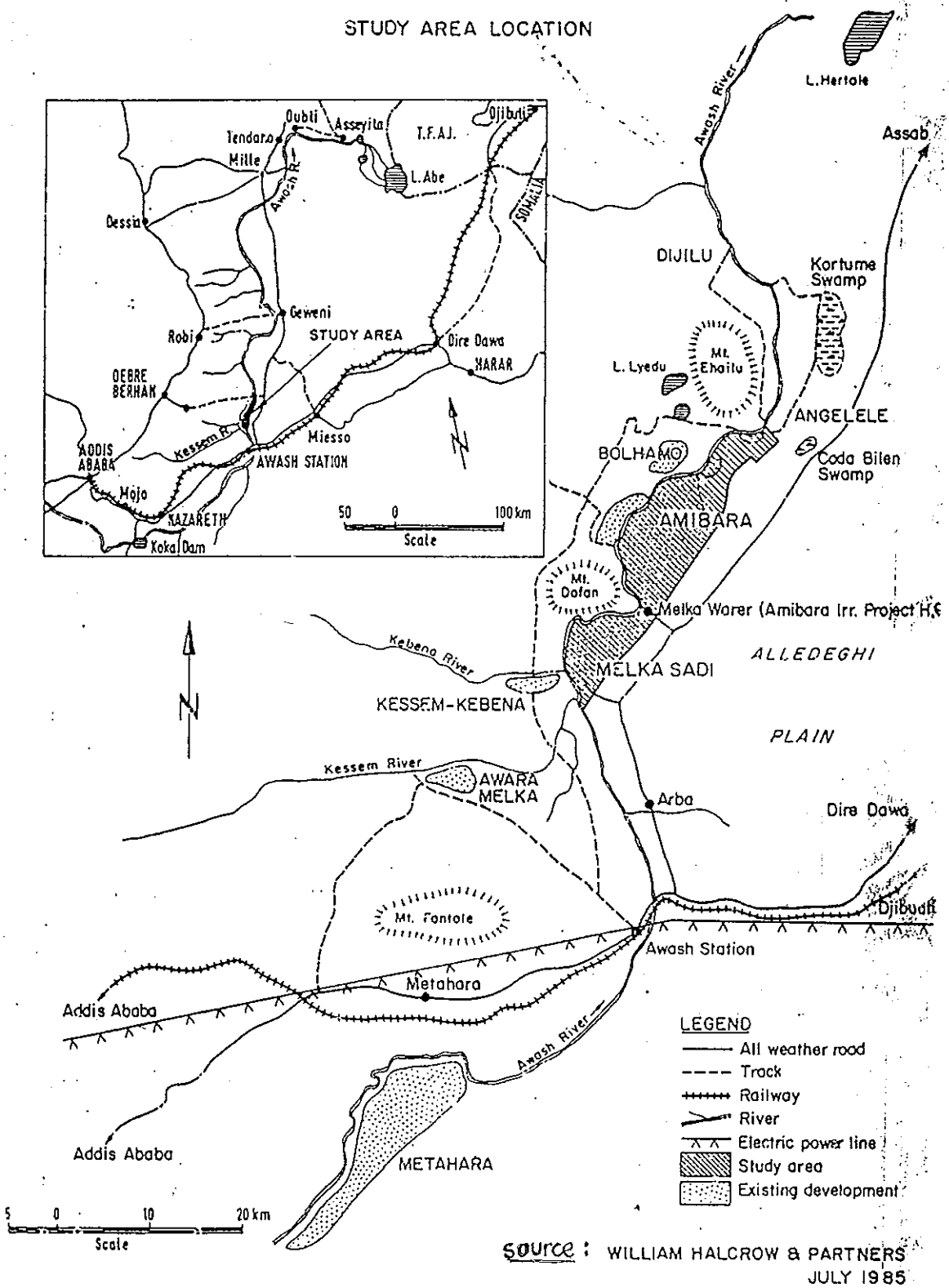

source : WILLIAM HALCROW & PARTNERS
JULY 1985

length of approximately 36 km. Gradients are generally very slight, predominantly lying in the range 0.5 to 1%.

To the east of the study area, the ground slopes gently away from the adjacent Aledeghi escarpment towards the north and north west, and a series of ill-defined drainage paths meander northwards through the study area towards the Angelele plains. The suppressed relief of the study area is interrupted occasionally by volcanic cinder cones, such as Amibara hill, which rise abruptly from the alluvial sequences of the flood plain. These provide evidence of recent volcanic activity in the area (Halcrow, 1986).

1.3.3 Types of production and source of irrigation water

The agricultural production under Amibara Irrigation Project (AIP), is based on the irrigation of cotton and bananas (at Melka Sadi only). The present gravity irrigation system which supplies the irrigated area postdates earlier pump arrangements in which irrigation water is lifted directly from the Awash river (Halcrow, 1985).

In a relatively short time after the commencement of AIP, yields of cotton and banana began to decline. The main reason identified in the early stages of the production decline was an increase in soil salinity levels (Dereje, 1992)

1.4 Previous Studies

The general geology of the area has been mapped by Halcrow (1975), during the feasibility study of Angelele-Bolhamo (Fig. 2)

During the feasibility study of the Melka Sadi –Amibara area, Italconsult (1969) had indicated he presence of a trough in the water table on the eastern side of the Awash alluvial plain. On either side of this trough, higher water table elevations were observed, indicating some

1.5 Objectives of the present study

The main objectives of this thesis work are to:

i. delineate or map the saline water and fresh water zones and the vertical and lateral variation of salinity.

ii. identify the general characteristics of the subsurface geology

iii. determine the depth of the aquifer/s and its/their salinity extent

iv. study the effectiveness of the resistivity method to delineate saline and fresh water zones

1.6 Methodology

The general procedures followed to achieve the above objectives were:

i. Areas, that are affected by salinity and convenient for the geophysical work, where there are adequate number of functioning observation wells along the traverses for controlling, were selected in the field.

ii. Geophysical data were collected applying electrical resistivity method (VES and profiling).

iii. Interpretations of field data were carried out and geoelectric sections and seudosections were plotted.

2. GEOLOGY AND HYDROGEOLOGY OF AMIBARA AREA

2.1 Geology

2.1.1 General Geology

The Main Ethiopian Rift (MER), separating the Ethiopian plateau to the west from the Somalian plateau to the east, runs NNE-SSW through the southern half of Ethiopia, and widens out northeastwards into the Afar. Both plateau rise to crests at the margins with rift system, chiefly due to upwarping towards the rifts (Mohr, 1967).

The MER-Southern Afar transition region, as defined by Chernet et al., (1998), is both an important physiographic and structural transition between the northern terminus of the MER and the southern-most Afar, and an important tectonic and volcanologic link between these two distinct manifestations of East African rifting. The physiographic transition occurs just north of Fantale where the narrow graben of the northern MER begin to funnel out into the Afar Depression. This transition is coincident with the intersection of the active, axial zone of modern rifting, the Wonji Fault Belt (WFB), and the circa E-W structures of the southern Afar marginal graben and Ambo Lineament which are extensions of the regional Gulf of Aden structural trend. Volcanic products that form the Nazareth Group cover an oval-shaped region centered around the central MER, and their distribution suggests that at least the lower members may be associated with the earliest stage of rifting. Nazareth group materials cover large portions of the rift margin and escarpments in the transition region (EIGS, 1978), and comprise a succession of welded ignimbrites, pumice, ash and rhyolite flows and domes with rare intercalation of basalt flows. The group attains a thickness of up to 200-250 m in the rift proper, and tends to thin out in the escarpments. Ignimbrites of the Nazareth group are considered to be products of eruptions mainly from marginal centers in the rift which have

been covered by more recent volcanocastic deposits (Morbidelli et al., 1973; Kazmin et al., 1980). Basaltic members of the Nazareth Group are less widespread and are exposed along faults forming the escarpments of the MER. Pre-rift basalt formations down-thrown into the rift floor are even less common, exposed only along fault scraps and deeply cut river gorges in the northern MER.

Widespread occurrences of upper Pliocene (4-1.6 Ma) basaltic volcanism in the northern MER are known by different names at different localities such as Wolenchiti Basalts (Mayer et al., 1975), Bishoftu Basalts and Rhyolites (Zanettin and Justin Visentin, 1974; Gasparon et al., 1993), and an Old Rift Floor basalts (UNDP, 1973). The name Bofa basalts was given by EIGS (1981) to all Pliocene rift floor basalts which are well exposed in the northern and central part of the MER and form a wedge between ignimbrites of the Nazareth and Wonji groups.

Several Quaternary trachytes to peralkaline rhyolite central volcanic complexes of Wonji groups also lie along the WFB in the northern MER-southern Afar transition region. Three segments of the WFB are present within the northern MER-southern Afar transition region, each hosting one or two major felsic centers: Boset and Kone in the southern-most segment, Fantale and Dofan in the central segment, and Ayelu (Mt. Ehailu) in the northern-most segment (Fig. 1). Recent activity at most of these centers is marked by obsidian flows, pumice/ash falls, and ignimbrite flows with rare scoreaceous basaltic flows (Chernet and Hart, 1999).

2.1.2 Local Geology of the Study Area

Amibara is found in the middle Awash valley, which lies in the northern sector of the MER of the tertiary age, extending northeast towards the Red Sea. Recent alluvial/colluvial

deposits from the Awash River and out wash from the escarpment are the main causes for the built up of the floor of the valley. Underlying sediments consist of nearly horizontal beds of basalts, pumice, gravel, tuffs, sands, silts and clays, and the latter are often saline.

Several features of volcanic origin are observed within the study area. A feature of the area is the low volcanic hills and cones at Amibara and Ambash, which,together with other minor extrusions, indicate the line of a fault running north-north east from Dofan (Halcrow, 1982)

As explained in the work of Dereje et al. (1996), these hills are surrounded by alluvial deposits. Both to the east and west, along the rift escarpment, there are slightly weathered volcanic outcrops. The volcanoes to the east are Miocene to Pleistocene fissures, dominantly basaltic flows associated with ignimbrites and rhyolites. To the west, the volcanoes are mostly silicic massif lava flow domes of ignimbrites and rhyolites, often peralkaline. Close to the eastern rift escarpment, parts of Arsi and Bale, there are wide outcrop basalts of Oligocene to upper Miocene age. Thc western escarpment and plateau margin is covered with Oligocene to Miocene undifferentiated volcanoes of the eastern margin of the central Ethiopian plateau (Kandiah, 1981).

A series of warm springs in the valley floor which form the Billen swamp are found north of the developed farm area. The water is alkali with an electrical conductivity of ± 0.1 mmhos/cm and probably enters the aquifer on the Alledeghi plain.

The present Awash river course, which is fault controlled, was formed in Plio-Pleistocene times; previously the river flowed in the Alledeghi graben to the south of its present course. This new course of the Awash was periodically blocked by lava flows or

outwash from the escarpment creating temporary lacustrine conditions. The valley floor was then some 50 meters below its present level (Halcrow, 1982).

According to Gezahegn (personal communication), Dofan (which is found adjacent to the present study area in the southwestern margin) is a small quaternary volcano found in neotectonic zone of the northern sector of the Ethiopian rift (latitude 9° 20′ N and longitude 40° 07′ E) where greater crustal attenuation has occurred.

2.1.3 Stratigraphy and evolution of Dofan volcanic center area

In the previous section it was stated that Dofan is situated at the southwestern margin of the study area. Therefore, explaining the stratigraphy of the vicinity of Dofan area is believed to be associated with the stratigraphy of Amibara area.

As explained in the work of Gezahegn (personal communication), the stratigraphy of the rift margin, nearest to Dofan, consists of Upper Miocene (15-13 Ma) rhyolites and basalts uncomformably covered by late Miocene – Pliocene (8-2 Ma) rhyolites belonging the Balchi formation (Zanettin and Jestin-Visentin, 1975). Volcanic series consisting of basalts and rhyolitic ignimbrites outcrops at the right margin to the west of Dofan (Chernet, and Gebre-egzaber, 1983), which correlate with the above mentioned formations.

A stratigraphic section that consists of basalts and ignimbrite units up to 400 meters thick, within the rift floor east of Dofan, characterized to the Afar Stratiod series (4.5-1 Ma) have been reported by Christiansen et al. (1975). At the Awash river gorge to the south of Dofan, Kazmin et al. (1980) have observed a thick series of silicic ignimbrites, collectively known us Nazareth Silicic Group, and overlain by a relatively thin basalt unit termed the Bofa Basalt. From these studies the northern sector of the Ethiopian rift floor is covered in its upper

part by a fairly continuous formation of silicic (ignimbrite) products and overlying basaltic units that predate the development of the Quaternary neotectonic belt and the associated volcanism.

Volcanic activity predating Dofan itself is represented by an ignimbrite unit of unknown thickness and an overlying basaltic layer of probable Quaternary age. These units are themselves covered by an important sedimentary sequence of fluvio-lacustrine origin that mantles this part of the rift floor and its western marginal areas (Chernet, and Gbre-egzabher, 1983). This sequences has been observed in outcrops immediately to the north of Dofan and clearly predate the products of the volcano. The exposed section here is formed of volcanoclastic sediments dominated by ash and pumice mixed with argillaceous clay and contains thin ash horizons towards its top. The section locally attains a thickness of about 40 meters in exposures along normal faults. An estimated thickness of about 100 meters has been reported by Elc-Geoterm Ital., (1987) for this unit further west nearer to the rift margin. It is thus logical to suppose that the sedimentary sequence is continuous beneath Dofan and evidences a period of relatively reduced volcanism prior to the onset of central volcanic activity.

The oldest volcanic products of Dofan so far recognized are represented by thin lava flows and associated cinder cones of intermediate and acidic composition outcropping as isolated patches in the external parts of the main edifice. The style of exposure of these units suggests that these earlier products were emitted from small vents located on NNE-SSW trending parallel fractures and probably underlies the main volcanic massif itself. These effusive products have given K-Ar ages of 1.7 Ma (Elc- Geoterm. Ital., 1987) and are the most mafic underlying rocks yet found at Dofan.

The youngest volcanic products at Dofan are represented by basaltic lava flows and associated scoria cones either contemporaneous with or postdating normal fault activity and clearly related to these younger structures.

The flood plain comprise of a complex sequence of silts, sandy silts and clays which have been laid in places to depths exceeding 100m. Towards the edges of the plain the infill grades into gravels and hillwash. Beyond the fault scarp lie the lava and gravel sequences of the Alledeghi. A number of basaltic and cinder cone intrusions through the alluvial layer indicate recent volcanic activity (Halcrow, 1986).

2.2 Hydrogeology

2.2.1 Climate

The mean annual temperature at Melka Werer meteorological station is 26.7 °C. The coldest months are November, December and January while the hottest is June. The average temperatures for all seasons are usually above 20 °C and the average night temperatures sometimes drop to 10 °C. At the same station the minimum monthly temperature reported was 11.8 °C in Nov. 1988, the maximum was 38.4 °C in May and June 1988.

The rainfall at Melka Werer Station is characterized by short rains in spring (small rainy season)– in most cases from the end of February to the end of April and long rains in summer (the big rainy season)– from July to August. The short rains do not fulfil the requirements for cropping in this area. These rather help to keep the relative humidity at a reasonable level by tempering the dryness of the plane. Generally, from the five years (1984 - 1988) rainfall data, it is observable that there is a variation of rainfall from one year to another and from one month to another. The rainfall recording at Melka Werer station shows that

against a minimum fall of 424.3 mm in 1984 there was a fall of 683.4 mm in 1988 (Dereje et al., 1996).

2.2.2 Aquifer system and recharge

The available drilling records show that all formations in the Awash River flood plain are water bearing. The sedimentary materials are consistently fine-grained and are characterized by a consistently low horizontal permeability. Aquifer type response is mainly the result of inflow from rainfall and irrigation and out flow by evaporation. Nevertheless, where boreholes have penetrated the gravel or fractured volcanics, water can be extracted in sufficient quantities for water supply purposes. Although confining layers may be encountered locally in the fine-grained sequences, the ground water is believed to be in hydraulic contact regardless of geological formations (Halcrow, 1985).

According to Halcrow (1982), there are two major aquifers in the area. The deeper aquifer which is saline and has shown a slow but general rise in level since observations were started in 1980. The recharge of this aquifer is supplied in part by infiltration upward from the underlying confined aquifers originating in the Alledeghi plain (Fig. 2). The Awash River at times of high flow, also contribute to this aquifer. A third possible contribution is the very saline ground water associated with the volcanic cones and features. The deep aquifer is receiving some water from the relatively shallow aquifer, which has developed since the introduction of irrigation, and this will continue to cause the aquifer to rise since the natural drainage towards the Billen swamp is extremely slow.

The shallow aquifer is generally of low salinity near the presently irrigated area and is gradually rising in level. At some sites it is extremely saline, particularly where the naturally saline ground water was already close to the surface as at Amibara and Ambash. The shallow

aquifer and the deep aquifer are separated by variable thickness of very slowly permeable or possibly impermeable clays and silty clays.

3. THEORETICAL AND MATHEMATICAL BASIS OF ELECTRICAL RESISTIVITY METHOD

A descriptive treatment of the more important aspects concerning on developing fundamental understanding of Electrical resistivity method and the physical principles on which it is based are discussed briefly in this section.

3.1 Basic idea and scope

In the electrical resistivity method a direct commutated or low frequency alternating current is introduced in to the ground by means of two electrodes (metal stakes) connected to the terminals of a portable source of electromotive force (emf). The resulting potential distribution on the ground, mapped by means of two probes (non-polarizable electrodes) is capable of yielding information about the distribution of electric resistivity below the surface.

3.2 Electric conduction in continuous media

The electric current in a short thin, linear conductor of uniform cross-section is given by Ohm's low

$$I = -\frac{dV}{R} \qquad (1)$$

where I is the current in Ampere (A), dV is the potential difference in volts (V) between the ends of the conductor and R is the resistance of the conductor in ohms (Ω). The minus sign expresses the fact that the current flow is from high to low potential (opposite to the increase of potential gradient).

Since resistance R is directly proportional to the length dl in meters (m) of the conductor and inversely proportional to the cross-sectional area A in square meters (m^2),

$$R = \rho \frac{dl}{A} \qquad (2)$$

where the constant of proportionality ρ is the resistivity in ohmmeters (Ωm) of the material of the conductor.

The distinction between resistance and resistivity is that resistance is a characteristics of a particular path of an electric current where as resistivity is a physical property of a material.

Substituting eqn. (2) in eqn. (1) for R and rearranging gives

$$\frac{I}{A} = -\frac{1}{\rho}\frac{dV}{dl} \qquad (3)$$

The left-hand side of eqn. (3) is the current density j (current per unit area of cross-section in A/m^2), while –dV/dl on the right hand side is the electric field E in V/m in the direction of the current density vector. Hence

$$j = \frac{E}{\rho} \qquad (4)$$

Since resistivity ρ is the inverse of conductivity σ in Siemens per meter (S/m) or mho per meter $(\Omega\ m)^{-1}$, eqn. (4) can alternatively be written as

$$j = \sigma E \qquad (5)$$

When the length dl in eqn. (3) tends to zero and if one considers the linear conductor as a homogeneous and isotropic continuous medium, then either of the eqns. (4) or (5) expresses Ohm's law for such a medium. Conductivity σ and resistivity ρ are independent of the direction of current flow in an isotropic medium (Parasnis, 1986).

3.3 Current flow in a homogeneous, Isotropic Earth

3.3.1 Point current source

The resistivity method consists of applying current and measuring potential P_1 when current is applied at a point source A. The return current electrode can be placed at a very great distance and assume material of uniform resistivity ρ. Because air has infinite resistivity, no current flows upward. Thus, current flows radially outward through the earth equally in all directions so as to define a hemispherical surface (Fig. 3). Since current distribution is equal every where on this surface, which is at a distance r from the current electrode A, the potential also is equal. These surfaces are known as equipotential surfaces.

By defining a very thin shell of thickness *dr* and employing eqn. (3), one can define the potential difference across the shell to be

$$dV = -I\rho\frac{dl}{A} = -I\rho\frac{dr}{2\pi r^2} \qquad (6)$$

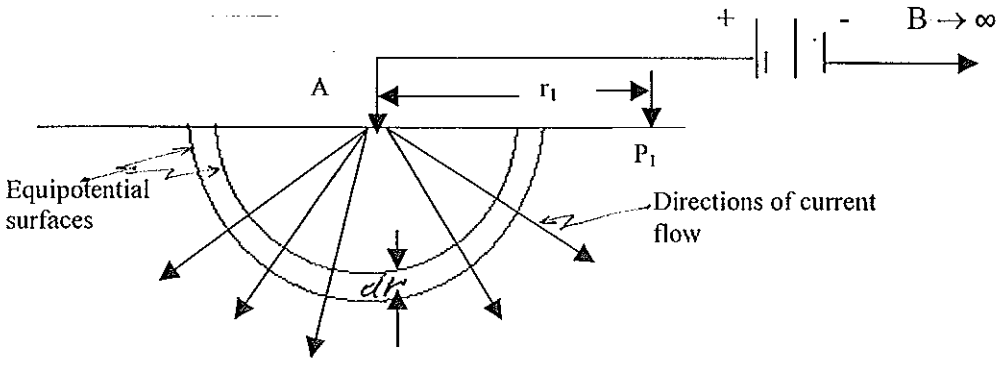

Fig. 3 Diagram illustrating symbols and configurations used to determine the potential at P_1 for a single point source of current A. The two equipotential surfaces shown are separated by the distance *dr*.

where dl = dr and $A=2\pi r^2$

Equation (6) determines the potential at P_1. The potential at a point infinitely far away by convention is arbitrarily defined to be equal to zero. The most direct way to determine V is to integrate eqn. (6) over its distance r_1 to the current electrode to infinity (Van Nostrand and Cook, 1966), or

$$V = \int_{r_1}^{\infty} dV = -\frac{I\rho}{2\pi}\int_{r_1}^{\infty}\frac{dr}{r^2} = \frac{I\rho}{2\pi r_1} \qquad (7)$$

This equations is the fundamental equation in Electrical resistivity prospecting discussions and it is possible to use it to develop more practical relationships as will seen in the following sections

The information, which can be obtained from eqn. (7) by assuming a resistivity and current is that, it enables to map the potential at any point in section view of figure 3. If adequate number of points were plotted one can draw lines through those points possessing the same potential. This defines the equipotential surfaces. Therefore, the direction of current flow can be determined, because current must be perpendicular to these equipotential surfaces.

3.3.2 Two current electrodes

In a homogeneous isotropic earth with two current electrodes the current must flow from the positive current electrode (the source) to the negative current electrode (the sink). The derivation for the case when the current electrodes and the potential point lie in the same plane as shown in figure 3 is that the potential at point P_1 is determined by using eqn. (7).

The effect of the source at A (+) and the sink at B (-) are both considered, and therefore.

$$V_{P_1} = \frac{I\rho}{2\pi r_1} + \left(-\frac{I\rho}{2\pi r_2}\right) = \frac{I\rho}{2\pi}\left(\frac{1}{r_1} - \frac{1}{r_2}\right) \qquad (8)$$

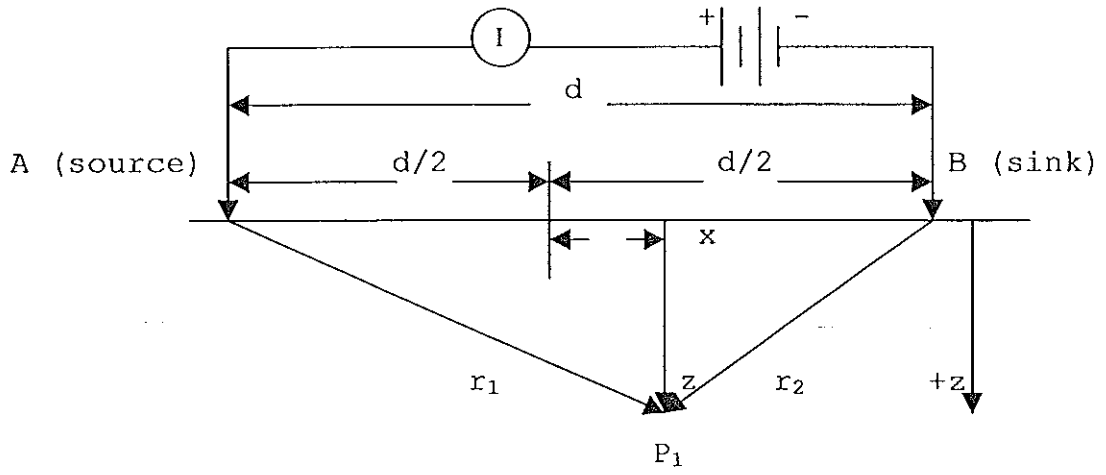

Fig. 4 Diagram illustrating symbols and configuration used to determine potential at P_1 for a current source A and sink B.

Expressing r_1 and r_2 in terms of x-z coordinate system shown in figure 4, eqn. (8) can be written as

$$V_{P_1} = \frac{I\rho}{2\pi}\left\{\frac{1}{\left[\left(\frac{d_2}{2}\right)^2 + z^2\right]^{\frac{1}{2}}} - \frac{1}{\left[\left(\frac{d_2}{2}\right)^2 + z^2\right]^{\frac{1}{2}}}\right\} \qquad (9)$$

This equation is used for a computer contouring package of the distribution of equipotential surfaces.

The current flow lines are perpendicular to the equipotential lines, but the manner in which current is distributed is not known. The mathematical analysis to determine the current distribution is fairly complicated but results in a simple equation that provides current

distribution as a fraction of the total current (Van Nostrand and Cook, 1966). Along a vertical plane midway between the two current electrodes (Fig. 4), the fraction of the total current I_f penetrating to depth z for an electrode separation d is given by (Burger, 1992)

$$I_f = 2\pi \tan^{-1}\left(\frac{2z}{d}\right) \qquad (10)$$

Current distribution for various current electrode separations can be investigated using eqn. (10). Therefore, for a homogeneous isotropic subsurface, the greater the electrode separation, the greater the depth to which a given percentage of current penetrates.

3.3.3 Two potential electrodes

The goal in electrical resistivity surveying is to measure the potential difference between two points. Figure 3 illustrates two potential electrodes M and N that are located on the surface as are the current electrodes. Using eqn. (8), derived to determine the potential at a point due to a source and a sink, the potential difference can be obtained by determining the potential at one potential electrode M and subtracting from it the potential at N.

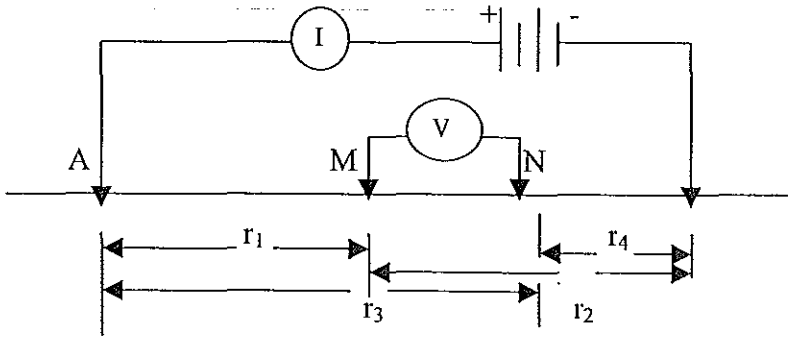

Fig.5 Diagram used to determine potential difference at two potential electrodes M and N.

Using eqn (8)

$$V_{P_1} = \frac{I\rho}{2\pi r_1} - \frac{I\rho}{2\pi r_2} \qquad (11)$$

and

$$V_{P_2} = \frac{I\rho}{2\pi r_3} - \frac{I\rho}{2\pi r_4} \tag{12}$$

Therefore the potential difference ΔV equals

$$\Delta V = V_{P_1} - V_{P_2} = \left(\frac{I\rho}{2\pi r_1} - \frac{I\rho}{2\pi r_2}\right) - \left(\frac{I\rho}{2\pi r_3} - \frac{I\rho}{2\pi r_4}\right) \tag{13}$$

or

$$\Delta V = \frac{I\rho}{2\pi}\left(\frac{1}{r_1} - \frac{1}{r_2} - \frac{1}{r_3} + \frac{1}{r_4}\right) \tag{14}$$

In resistivity method, a known current is entered into the ground, potential difference is measured, and resistivity can be determined. Because resistivity is the unknown quantity, one can solve for the resistivity ρ from eqn (14) and obtain (Burger, 1992)

$$\rho = 2\pi \frac{\Delta V}{I}\left(\frac{1}{r_1} - \frac{1}{r_2} - \frac{1}{r_3} + \frac{1}{r_4}\right)^{-1} \tag{15}$$

3.3.4 Apparent resistivity

Before discussing the various electrode spreads, it is necessary to consider what is actually measured by any array of current and potential electrodes. From eqn. (15)

$$\rho = K\frac{\Delta V}{I} \tag{16}$$

where

$$K = 2\pi\left(\frac{1}{r_1} - \frac{1}{r_2} - \frac{1}{r_3} + \frac{1}{r_4}\right)^{-1}$$

is the geometric parameter, which depends on the electrode disposition.

By measuring ΔV and I and knowing the electrode configuration, one obtains the resistivity ρ. Over homogeneous isotropic ground the resistivity will be constant for any

current electrode arrangement. For non-homogeneous ground, however, as the electrode spacing is varied, or the spacing remains fixed while the whole array is moved, then the ratio will in general change. This results in a different value of ρ for each measurement. The magnitude is intimately related to the arrangement of electrodes. This measured quantity is known as the *apparent reresistivity* ρ_a. Although it is diagnostic to some extent of the actual resistivity of a zone in the vicinity of the electrode array, the apparent resistivity is definitely not an average value and only in the case of homogeneous grounds it is equal to the actual resistivity (Telford et al., 1990).

3.4 Potential of a point current electrode on the surface of a horizontally-layered earth

To find a practical method of determining the resistivities of the layers and the depths of the boundary planes from the potential differences that are measured at the surface of the earth, one has to know the fundamental mathematical relation between the measured quantities the parameters that define the layer distribution in the surface derived by Stefanesco et al., (1930).

The problem can be simplified by assuming:

- the potential to be generated by a point source of current
- the potential field about the vertical axis of the current source is axially symmetric and the potential is additive

Problem formulation

- the subsurface consists of a finite number of layers separated by horizontal boundary planes; the deepest layer extending to infinite depth, while the other layers have finite thickness, that means $h_n \rightarrow \infty$, $h_i = h_1, h_2, h_3 \ldots h_{n-1}$
- each of the layers are electrically homogeneous and isotropic

- the field is generated by a point source of current located at the surface
- the current source is direct current

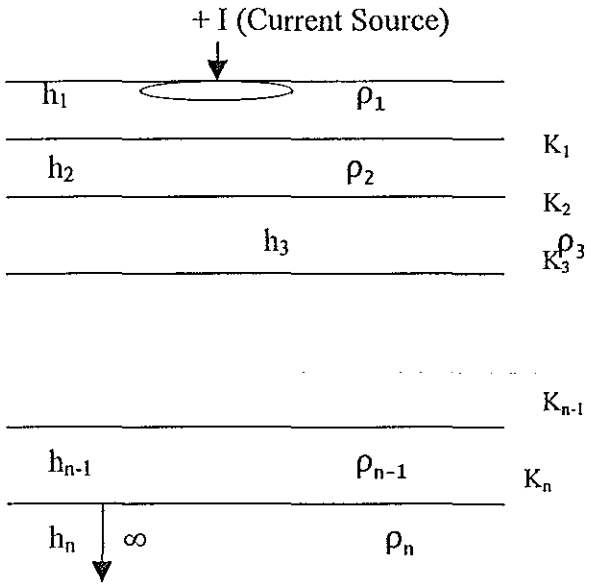

Fig. 6 Point electrode on a stratified earth and the cylindrical coordinate system.

The electrical potential V for DC satisfies the differential equation of Laplace

$$\nabla^2 V = 0 \qquad (16)$$

That means, $\frac{\partial^2 V}{\partial^2 x} + \frac{\partial^2 V}{\partial^2 y} + \frac{\partial^2 V}{\partial^2 z} = 0$ (in Cartesian coordinates)

Since the potential field has a cylindrical symmetry about the vertical axis passing through the point delivering the current, one should preferably use Laplace equation in cylindrical coordinates

$$\frac{\partial^2 V}{\partial r^2} + \frac{1}{r}\frac{\partial V}{\partial r} + \frac{\partial^2 V}{\partial z^2} + \frac{1}{r^2}\frac{\partial^2 V}{\partial \theta^2} = 0 \qquad (17)$$

For a solution symmetrical with respect to the vertical axis, $dV/d\theta = 0$ and $d^2V/d\theta^2 = 0$, so that eqn. (17) becomes

$$\frac{\partial^2 V}{\partial r^2}+\frac{1}{r}\frac{\partial V}{\partial r}+\frac{\partial^2 V}{\partial z^2}=0 \qquad (18)$$

The particular solution of eqn. (18) is obtained by the method of separation of variables

$$V(r,z) = U(r)\, W(z) \qquad (19)$$

Substituting eqn. (19) into eqn. (18) yields

$$W(z)\frac{d^2U(r)}{dr^2}+\frac{1}{r}W(z)\frac{dU(r)}{dr}+U(r)\frac{d^2W(z)}{dz^2}=0$$

dividing throughout by U(r) W(z) gives

$$\frac{1}{U(r)}\frac{d^2U(r)}{dr^2}+\frac{1}{r}U(r)\frac{dU(r)}{dr}+\frac{1}{W(z)}\frac{d^2W(z)}{dz^2}=0 \qquad (20)$$

eqn. (20) is satisfied if and only if

$$\frac{1}{U(r)}\frac{d^2U(r)}{dr^2}+\frac{1}{r}U(r)\frac{dU(r)}{dr}=-\lambda^2 \qquad (21)$$

and

where λ is arbitrary constant

The solution of eqn. (21) is

$$U(r)=C_1J_0(\lambda r) \qquad (23)$$

where J_O is Bessel function of order zero.

The solutions of eqn. (22) can be written as

$$W(z)=C_2e^{-\lambda z} \qquad \text{and} \qquad W(z)=C_3e^{+\lambda z} \qquad (24)$$

By the theory of differential equation, if eqns. (23) and (24) are solutions of eqn. (18), then their combination is also a solution.

$$V(r,z) = Ce^{-\lambda z}J_0(\lambda r) \qquad (25)$$
$$V(r,z) = Ce^{+\lambda z}J_0(\lambda r)$$

where C and λ are arbitrary constants

Since the linear combination of eqns. (25) are also solutions, making to go through all possible values from $0 \rightarrow \infty$ and allowing the two constants "C" to vary independent of λ,the general solution of eqn. (18) is obtained as

$$V(r,z) = \int_0^\infty \left[\phi(\lambda)e^{-\lambda z} + \psi(\lambda)e^{+\lambda z}\right]J_0(\lambda r)d\lambda \qquad (26)$$

From the basic theory of the potential generated by a point source of current of intensity I placed at the surface of an electrically homogeneous semi- infinite earth (analogous to eqn. 7),

$$V(r,z) = \frac{I\rho}{2\pi}\left[\frac{1}{\sqrt{r^2+z^2}}\right] \qquad (27)$$

To write eqn (27) in integral form, we can use Weber integral (Lipschitz integral) formula, that is

$$\left[\frac{1}{\sqrt{r^2+z^2}}\right] = \int_0^\infty e^{-\lambda z}J_0(\lambda r)d\lambda \qquad (28)$$

so that eqn. (27) is written as

$$V(r,z) = \frac{I\rho}{2\pi}\int_0^\infty e^{-\lambda z}J_0(\lambda r)d\lambda \qquad (29)$$

Equation (29) is also a solution for eqn. (18). Hence, the general solution is given by

$$V(r,z) = \frac{I\rho}{2\pi}\int_0^{\infty}\left[e^{-\lambda z} + \theta(\lambda)e^{-\lambda z} + \chi(\lambda)e^{+\lambda z}\right]J_0(\lambda r)d\lambda \qquad (30)$$

where $\theta_i(\lambda)$ and $\chi_i(\lambda)$ are arbitrary functions of λ

The solutions of eqn. (30) are valid for each of the subsurface layers (the functions $\theta_I(\lambda)$ and $\chi_i(\lambda)$ may not take the same form in each of the layers). Therefore, for each of the layers in the subsurface the potential must satisfy

$$V_i(r,z) = \frac{I\rho_i}{2\pi}\int_0^{\infty}\left[e^{-\lambda z_I} + \theta_i(\lambda)e^{-\lambda z_I} + \chi_i(\lambda)e^{+\lambda z_I}\right]J_0(\lambda r)d\lambda \qquad (31)$$

Equation (31) is called Stefanesco integral and "i" refers to several layers of the sub surface (Koefoed, 1968)

Boundary conditions to solve eqn. (31) are:

i) The potential at each of the boundary planes must be continuous. That means

$$V_i = V_{i+1} \quad \text{at} \quad z = h_i \qquad (32)$$

ii) The current density normal to each interface must be continuous. That means

$$\frac{1}{\rho_i}\frac{\partial V_i}{\partial z} = \frac{1}{\rho_{i+1}}\frac{\partial V_{i+1}}{\partial z} \qquad at \qquad z = h_i \qquad (33)$$

$(j_i)_n = (J_i)_{n+1}$ and since $j = \sigma E = \frac{1}{\rho}\frac{\partial V}{\partial z}$

iii) At the surface ($z = 0$) the vertical component of the potential must be zero everywhere except at infinitesimal neighborhood around the current source (because of condition (ii) and $j = 0$)

iv) At the surface and near the current source, the potential has to be finite.

$$V = \frac{I\rho}{2\pi}\frac{1}{\sqrt{r^2 + z^2}}$$

at $z = 0$ and as r approaches 0, the result of this expression is finite.

v) From eqn. (27) at infinite depth, the potential must reduce to zero. That means,

$$V \to 0 \quad \text{as} \quad z \to \infty \tag{34}$$

Applying these boundary conditions to eqn (31),

From condition (i)

$V_i = V_{i+1}$ at $z = h_i$

$$\int_0^\infty \left[e^{-\lambda h_i} + \theta_i(\lambda)e^{-\lambda h_i} + \chi_i(\lambda)e^{+\lambda h_i}\right] J_0(\lambda r) = \int_0^\infty \left[e^{-\lambda h_i} + \theta_{i+1}(\lambda)e^{-\lambda h_i} + \chi_{i+1}(\lambda)e^{+\lambda h_i}\right] J_0(\lambda r)$$

This equation can be satisfied for all values of r if the integrands on both sides are equal.

$$\theta_i(\lambda)e^{-\lambda h_i} + \chi_i(\lambda)e^{+\lambda h_i} = \theta_{i+1}(\lambda)e^{-\lambda h_i} + \chi_{i+1}(\lambda)e^{+\lambda h_i} \tag{35}$$

$$\frac{1}{\rho_i}\int_0^\infty \left[(1+\theta_i(\lambda))e^{-\lambda h_i} - \chi_i(\lambda)e^{+\lambda h_i}\right] J_0(\lambda r)\lambda d\lambda = \frac{1}{\rho_{i+1}}\int_0^\infty \left[(1+\theta_{i+1}(\lambda))e^{-\lambda h_i} - \chi_{i+1}(\lambda)e^{+\lambda h_i}\right] J_0(\lambda r)\lambda d\lambda$$

From condition (ii)

$$\frac{1}{\rho_i}\frac{\partial V_i}{\partial z} = \frac{1}{\rho_{i+1}}\frac{\partial V_{i+1}}{\partial z}$$

The above condition is satisfied if and only if,

$$\frac{1}{\rho_i}\left[(1+\theta_i(\lambda))e^{-\lambda h_i} - \chi_i(\lambda)e^{+\lambda h_i}\right] = \frac{1}{\rho_{i+1}}\left[(1+\theta_{i+1}(\lambda))e^{-\lambda h_i} - \chi_{i+1}(\lambda)e^{+\lambda h_i}\right] \tag{36}$$

From condition (iii)

When eqn. (31) is differentiated with respect to z and evaluated at z = 0, it gives

$$\int_0^\infty \left[-1 - \theta_1(\lambda) + \chi_1(\lambda)\right] J_0(\lambda r)\lambda d\lambda = 0 \tag{37}$$

$$\frac{1}{\rho_1}\left[(1+\theta_1)u_1 - \theta_1 v_1\right] = \frac{1}{\rho_2}\left[(1+\theta_2)u_1 - \chi_2 v_1\right]$$

$$(v_1 - u_1)\theta_1 + p_1 u_1 \theta_2 - p_1 v_1 \chi_2 = (1 - p_1)u_1 \qquad (41)$$

For i = 2

Equation (35) becomes,

$$u_2\theta_2 + v_2\chi_2 - u_2\theta_3 - v_2\chi_3 = 0 \qquad (42)$$

Equation (36) becomes,

$$-u_2\theta_2 + v_2\chi_2 + p_2 v_2\theta_3 - p_2 v_2\chi_3 = (1 - p_2)u_2 \qquad (43)$$

It continues in the same manner up to i = n -1 and,

For i = n-1

Applying the condition of eqn. (39), eqn. (35) becomes

$$u_{n-1}\theta_{n-1} + v_{n-1}\chi_{n-1} - u_{n-1}\theta_n = 0 \qquad (44)$$

and eqn. (36) becomes

$$u_{n-1}\theta_{n-1} + v_{n-1}\chi_{n-1} + p_{n-1}u_{n-1}\theta_n = (1 - p_{n-1})u_{n-1} \qquad (45)$$

The solution of these systems of equations for θ_1, is obtained by Cramer's rule. According to this rule θ_1, is obtained as a quotient of two determinants. The denominator is the determinant of the matrix that is formed by the coefficient of θ and χ on the left hand side of the equations of the system. The numerator is the determinant of the same matrix with the elements of the first column replaced by the coefficients on the right hand side of the equations of the system. Thus the denominator matrix D is the following

$$D = \begin{pmatrix} (u_1 + v_1) & -u_1 & -v_1 & & & & & \\ (v_1 - u_1) & p_1 u_1 & -p_1 v_1 & & & & & \\ & u_2 & v_2 & -u_2 & -v_2 & & & \\ & -u_2 & v_2 & p_2 u_2 & -p_2 v_2 & & & \\ & . & . & . & . & & & \\ & . & . & . & . & & & \\ & & & & & u_{n-1} & v_{n-1} & -u_{n-1} \\ & & & & & -u_{n-1} & v_{n-1} & p_{n-1} u_{n-1} \end{pmatrix} \tag{46}$$

and the numerator matrix is denoted by

$$P = \begin{pmatrix} 0 & -u_1 & -v_1 & & & & & \\ (1-p_1)u_1 & p_1 u_1 & -p_1 v_1 & & & & & \\ 0 & u_2 & v_2 & -u_2 & -v_2 & & & \\ (1-p_2)u_2 & -u_2 & v_2 & p_2 u_2 & -p_2 v_2 & & & \\ & & . & . & . & & & \\ & & . & . & . & & & \\ & & . & . & . & & & \\ & & & & & u_{n-1} & v_{n-1} & -u_{n-1} \\ & & & & & -u_{n-1} & v_{n-1} & p_{n-1} u_{n-1} \end{pmatrix} \tag{47}$$

where

$$\theta_1 = \frac{|P|}{|D|} \tag{48}$$

The determinant P can be simplified by adding the second column to all the elements of the first column (which does not change the determinant). This yields a matrix of the following type:

$$P = \begin{pmatrix} -u_1 & -u_1 & -v_1 & & & & \\ u_1 & p_1u_1 & -p_1v_{11} & & & & \\ u_2 & u_2 & v_2 & -u_2 & -v_2 & & \\ -p_2u_2 & -u_2 & v_2 & p_2u_2 & -p_2v_2 & & \\ & & & & \cdot & & \\ & & & & \cdot & & \\ & & & & \cdot & & \\ & & & & & u_{n-1} & v_{n-1} & -u_{n-1} \\ & & & & & -u_{n-1} & v_{n-1} & p_{n-1}u_{n-1} \end{pmatrix} \qquad (49)$$

Example for a two layer case

The matrix D and P for a two-layer case are:

$$P = \begin{pmatrix} -u_1 & -u_1 \\ u_1 & p_1u_1 \end{pmatrix} \qquad D = \begin{pmatrix} u_1 + v_1 & -u_1 \\ v_1 - u_1 & p_1\,u_1 \end{pmatrix}$$

$$P = (1-p_1)u_1^{\,2} \qquad \text{and} \qquad D = p_1u_1^{\,2} + p_1u_1v_1 + u_1v_1 - u_1^{\,2}$$

$$u_1 = \frac{1}{v_1} \qquad D = (1+p_1) - (1-p_1)u_1^{\,2}$$

and

Since
$$\theta_i(\lambda) = \frac{(1-p_1)u_1^{\,2}}{(1+u_1) - (1-p_1)u_1^{\,2}} = \frac{(1-p_1)u_1^{\,2}/(1+p_1)}{1-(1-p_1)u_1^{\,2}/(1+p_1)}$$

or

Substituting the values previously set for u and p in this equation yeilds,

$$\theta_1 = \frac{k_1e^{-2\lambda h_1}}{1-k_1e^{-2\lambda h_1}} \qquad (49')$$

where

$$k_1 = \frac{1-p_1}{1+p_1} = \frac{\rho_2 - \rho_1}{\rho_2 + \rho_1}$$

is the reflection coefficient of the first interface.

3.4.1 The Kernel Function and its relation to subsurface parameters

For the top most layer, the Stefanesco integral of eqn. (31) when $\theta_1(\lambda) = \chi_1(\lambda)$ and z = 0 becomes

$$V = \frac{I\rho_1}{2\pi}\int_0^\infty [1 + 2\theta_1(\lambda)]J_0(\lambda r)d\lambda \qquad (50)$$

Since,

$$\frac{1}{\sqrt{r^2+z^2}} = \int_0^\infty e^{-\lambda z} J_0(\lambda r)d\lambda$$

from eqn. (28) and at z = 0, $\frac{1}{r} = \int_0^\infty J_O(\lambda r)d\lambda$

it is the potential at the surface of the earth satisfying the specified conditions.

Let

$$k(\lambda) = 1 + 2\theta_1(\lambda)$$

or eqn. (51) can be written as,

$$V = \frac{I\rho_1}{2\pi}\left\{\frac{1}{r} + 2\int_0^\infty \theta_1(\lambda)J_0(\lambda r)d\lambda\right\} \qquad (52)$$

Because as mentioned , $\frac{1}{r} = \int_0^\infty J_O(\lambda r)d\lambda \quad for \quad z = 0$

In eqns. (50) and (51), $\theta_1(\lambda)$ is called the Stefanesco Kernel Function and $k_1(\lambda)$ introduced into resistivity theory by Slichter (1933) is called the Slichter Kernel Function.

$$\left(\frac{\partial V_S}{\partial r}\right)_{r=s} = -\frac{\rho_1 I}{\pi}\left\{\frac{1}{s^2} + 2\int_0^\infty \theta(\lambda) J_1(\lambda s)\lambda d\lambda\right\} \qquad (55)$$

From the relation of the potential for homogeneous earth discussed in section 3.3, denoting the apparent resistivity for Schulmberger configuration by ρ_{as}, from eqn. (55)

$$V_\rho = \frac{I\rho}{2\pi r} \quad and \quad \left(\frac{\partial V_s}{\partial r}\right)_{r=s} = -\frac{\rho I}{\pi s^2} \qquad (56)$$

Substituting eqn. (54) in eqn. (55) yields (Koefoed, 1968)

$$\rho_{aS} = \frac{-\pi s^2}{I}\left(\frac{\partial V_S}{\partial r}\right)_{r=s} \qquad (57)$$

$$\rho_{aS} = \rho_1\left\{1 + 2s^2\int_8^\infty \theta(\lambda) J_1(\lambda s)\lambda d\lambda\right\} \qquad (58)$$

The Resistivity Transform

The Kernel Function of resistivity, from equation (52) and the theory of Bessel functions and putting

$$V = \frac{I\rho_1}{2\pi}\left\{\int_0^\infty J_0(\lambda r) + 2\int_0^\infty \theta(\lambda) J_0(\lambda r) d\lambda\right\}$$

$$Since \quad \frac{1}{r} = \int_0^\infty J_0(\lambda r) d\lambda$$

$$V = \frac{I\rho}{2\pi}\frac{1}{r}\left\{1 + 2r\int_0^\infty \theta(\lambda) J_0(\lambda r) d\lambda\right\} \qquad (59)$$

$$T(\lambda) = \rho_1[1 + 2\theta(\lambda)]$$

empirical relationship due to Archie for the dependence of the resistivity on the porosity and fluid resistivity is given by

$$\rho_e = a\phi^{-m}s^{-n}\rho_w \qquad (62)$$

where ϕ - is the fractional pore volume (porosity),

s - is the fraction of the pores containing water,

ρ_e - is the bulk resistivity,

ρ_w - the resistivity of pore fluid (water),

m - is the cementation factor, $1.3 < m < 2.5$ and $0.5 < a < 2.5$, $n \cong 2$, (a, n and m are constants in the specified range)

Increasing cementation usually decreases the porosity and therefore also increases the formation factor as well as the bulk resistivity. All resistivity-sensing, surface-electrical methods detect the bulk resistivity of a volume of rock at depth (in situ) with resistivity values reflecting the combined effects of all conduction modes. The range of resistivities among rocks is quite large, extending from under 10^{-2} to 10^{8} Ωm and above. Rocks and minerals with resistivities below 1.0 Ωm are considered good conductors; those from 1 to 100 Ω m, intermediate conductors; and those from 100 and up, poor conductors. Table 1 lists the ranges within which resistivity have been observed for several types of water-bearing rocks.

Table 1 Resistivities (in Ohmmeters) for water-bearing rocks of various types (Keller, 1966)

Geologic age	Marine Sand, Shale, Graywacke	Terrestrial Sands, claystone, arkose	Volcanic rocks (basalt, rhyolite, tuffs)	Granite, gabbro, etc.	Limestone, Dolomite, Anhydrite, Salt
Quatemary,	1-10	15-50	10-2000	500-2000	50-5000
Tertiary	5-20	25-100	20-500	500-2000	100-10,000
Mesozoic	10-40	50-300	50-1000	1000-5000	200-100,000
Carboniferous	40-200	100-2000	100-2000	1000-2000	10,000-
Pre-carboniferous					100,000
Paleozoic	300-5000	200-5000	200-5000	5000-	
Precambrian				20,000	10,000-
					100,000

3.6 Common electrode configurations

In actual practice a number of different conventional surface configurations are used for the current and potential electrodes. In many arrangements, both sets of electrodes are laid out along a line. The current electrodes are generally placed on the outside of the potential electrodes (symmetrical). The most widely used configurations will be described in the

paragraphs that follow. For convenience V will denote the measured voltage while the potential difference is denoted by ΔV.

Wenner array

One common electrode arrangement for resistivity measurement is the Wenner configuration illustrated in figure 7a. Here each potential electrode is separated from the adjacent current electrode by a distance *a,* which is one-third the separation of the current electrodes. For this arrangement, setting $r_1 = r_4 = a$ and $r_2 = r_3 = 2a$ in eqn (15),the apparent resistivity becomes

$$\rho_a = 2\pi a \frac{\Delta V}{I} \qquad (63)$$

The Wenner arrangement is a special case of the Schlumberger array, discussed next.

Schlumberger array

In the Schlumberger configuration, the operator expands the electrode spacing by increasing the distance between current electrodes, typically on a logarithmic scale, during the course of a measurement. The potential-electrode spacing is assumed to be infinitesimal, and the observed values of potential can be adjusted accordingly. The Schlumberger electrode arrangement is illustrated in figure 7b.

The apparent resistivity at the center of a Schlumberger array, $r_1 = r_4 = (s - a/2)$ and $r_2 = r_3 = (s + a/2)$ in eqn. (15) yields

$$\rho_a = \pi \frac{\left(s^2 - a^2/4\right)}{a} \frac{\Delta V}{I} \qquad (64)$$

where s is half of the current-electrode separation (i.e., AB/2). The separation '*a*' between the potential electrodes MN is typically very small. For a "point dipole," eqn. (64) becomes

$$\rho_a = \frac{\pi s^2}{a}\frac{\Delta V}{I} \qquad (65)$$

As a practical matter, when one considers attainable instrument accuracy, $a < 0.05s$ is sufficient and eqn. (65) can be used to compute the apparent resistivity from the field measurements of ΔV and I versus current-electrode spacing, s.

Dipole array

The dipole methods, more recently introduced than the Wenner or Schlumberger methods, are widely used, especially in the U.S.S.R., for deep penetration. Such a dipole-dipole array is illustrated in figure 7c. The current electrodes are usually well separated from the potential electrodes. If the separations a and b are equal and the distance between the centers of the respective pairs is (n+1) a, the apparent resistivity determined by this arrangement by setting $r_1 = r_4 = (n+1)\,a$, $r_2 = na$ and $r_3 = (n+2)\,a$ in eqn. (15) yields

$$\rho_a = n\,(n+1)\,(n+2)\;\pi a\frac{\Delta V}{I} \qquad (66)$$

Another collinear dipole arrangement is the pole-dipole shown in figure 7d. The second current electrode, B, is assumed to be at a great distance from the measurement location (infinite position for the second electrode). For this configuration

$$\rho_a = 2\pi a\, n\,(n+1)\frac{\Delta V}{I} \qquad (67)$$

If one of the potential electrodes, N, is also at a great distance, the configuration is called pole-pole figure 7e. The apparent resistivity is then

$$\rho_a = 2\pi a \frac{\Delta V}{I} \qquad (68)$$

The apparent resistivities from dipole arrays are commonly plotted on a pseudo cross section along the traverse of measurements. Such a section cannot be analyzed as a vertical section showing resistivity variations. The apparent resistivity, $_a$, va lues are plotted at the midpoint between the current transmitter and the potential (voltage) receiver. The vertical axis corresponds to n, the separation parameter (Dobrin et. al., 1988).

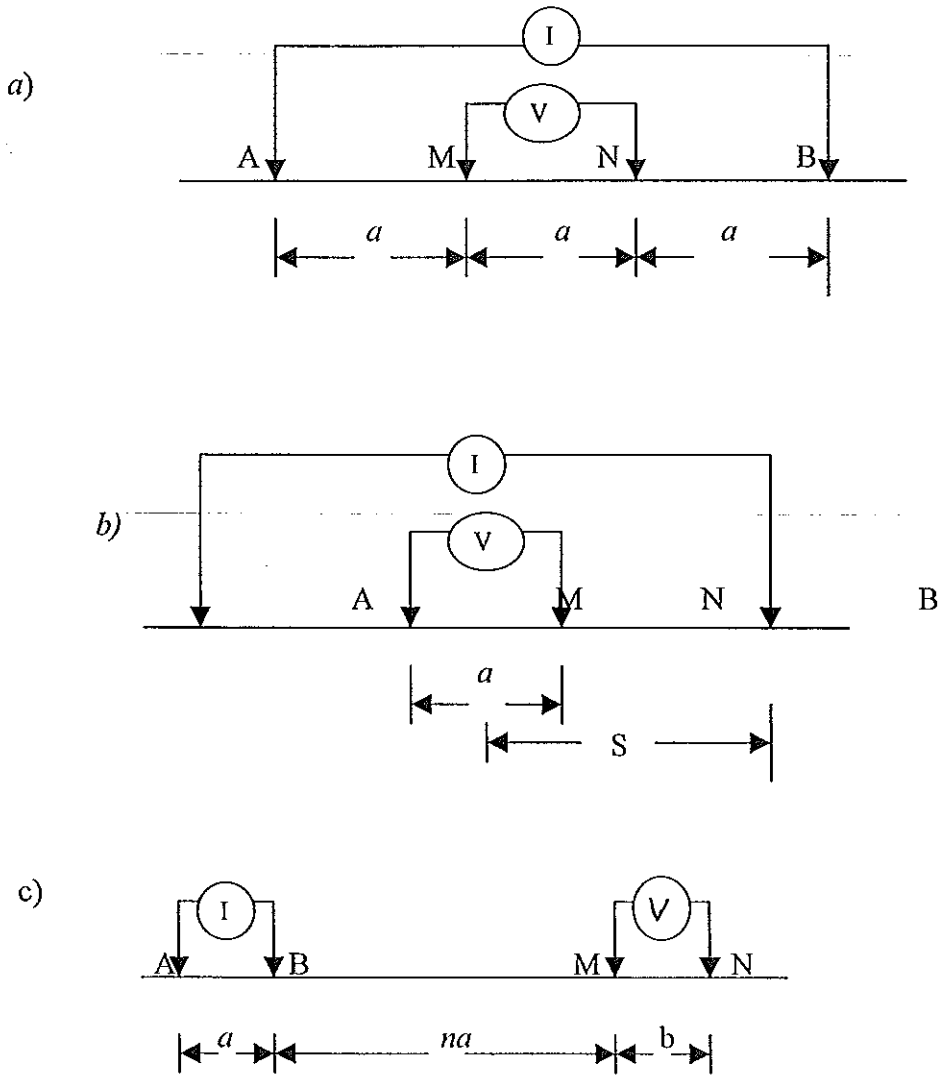

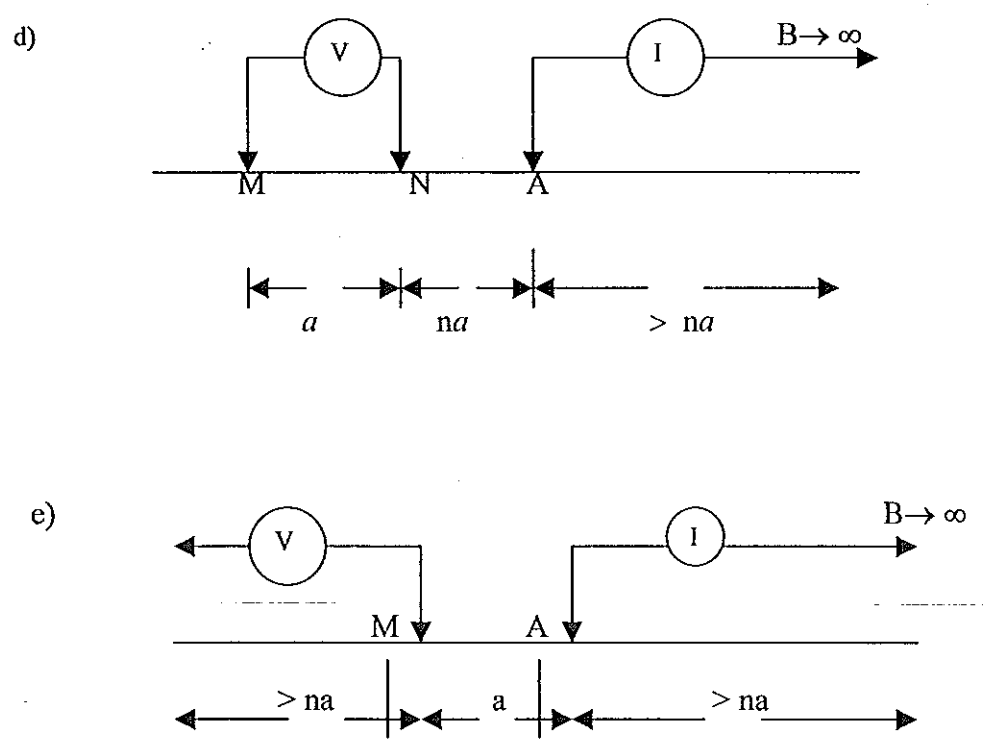

Fig.7 Collinear electrode configurations in common use: a) Wenner; b) Schlumberger; c) dipole –dipole (axial); d) pole-dipole; e) pole-pole. For all arrays A and B are current electrodes while M and N are potential electrodes.

3.7 Resistivity field survey procedures

The two basic procedures to be used in resistivity work, depending on whether one is interested in resistivity variation with depth or with lateral extent respectively are Vertical Electrical Sounding (VES) and lateral profiling.

3.7.1 Vertical Electrical Sounding

Since the fraction of total current that flows at depth varies with the current electrode separation, as described in section 3.3.2, the field procedure is to use a fixed center with an

expanding spread. Although the pole-dipole array is not suited to this technique, any of the other three configurations (Wenner, Schlumberger and Dipole-dipole) may be used.

The Schlumberger array is best used for VES, because the potential electrodes remain fixed while the current electrode spacing is expanded symmetrically about the center of the spread. For large value of AB/2 it may be necessary to increase MN/2 also in order to maintain a measurable potential. This procedure is more convenient than the Wenner expanding spread because only two electrodes need move at a time. In addition, the effect of shallow resistivity variations is constant with fixed potential electrodes.

The presence of horizontally or gently dipping beds of different resistivities is best detected by the expanding spread. Hence the method is useful in determining depth of overburden; depth, structure, and resistivity of flat-lying sedimentary beds and possibly of the basement also if it is not too deep.

It is frequently necessary to carryout this expansion procedure at several locations in an area, even when the main interest may be in lateral exploration, to establish the proper electrode spacing for the lateral search (Telford et al., 1990).

3.7.2 Lateral profiling

Resistivity profiling is particularly useful in mineral exploration, where the detection of isolated bodies of anomalous resistivity is required. It is also used in studying steeply dipping contacts (faults, dikes, shear zones and steeply dipping veins), or for lateral changes in the resistivity of a particular horizon. In resistivity profiling, the spacing between the electrodes is held constant, and the array is moved as a whole along the traverse line. Apparent resistivity is plotted against the mid point of the potential electrodes for symmetrical arrays (Telford et al., 1990; Keller and Frischknecht, 1966).

A given distance between current and potential electrodes corresponds to a set of data related to a nearly constant depth of investigation, and thus to a layer of earth of a given thickness. The dimensions of the configuration will then be chosen as a function of the depth of the problem in question. The succession of resistivity, determined by electrical sounding and calibrated if possible by drilling also has to be considered. To correctly interpret the results, maps based on several length of configuration may be necessary

Any one of the configurations (Wenner, Schlumberger or Dipole-dipole) can be used to establish resistivity profiles or maps. To this end, one must either move the complete configuration after each measurement or cause the electrodes MN to occupy a serious of different positions between each movement of the current electrodes AB. In both cases, the group of measurements will correspond to the same depth of investigation or to several, nearly constant values of that depth.

The two quadripoles by far the most used (Figs. 7*a* and 7b) are still the Wenner configuration, in which the electrodes are equally spaced, and the Schlumberger configuration, in which the distance MN is small with respect to the distance AB, generally smaller than AB/5. With the latter configuration the ratio of the potential difference to the interval MN is practically equal to the field strength near the center .of the configuration, since the field is nearly uniform in the neighborhood of this point.

Among the quadripoles in which MN is exterior to AB, the only ones that are not imperfect tripoles (when the configuration is asymmetrical and MN is much nearer one of the current electrodes, it is called imperfect tripole) are those in which the intervals MN and AB are both small with respect to the separation between them (Fig 7c). Such a configuration is called a Dipole-dipole. The advantage of this configuration is that it requires much less cable for a given depth of investigation than do other configurations.. The disadvantage is the

comparatively low potential difference between the electrodes MN for a given value of the applied current and the preponderant role played by the nature of the terrain near the current electrodes AB. In fact, the potential difference varies inversely as the cube of the distance between the current electrodes and the potential electrodes in this configuration where as in the Schlumberger configuration it varies inversely as the square of the electrode interval AB.

Use of several line lengths

Measurements with a single electrode separation may often be insufficient, even more so since the depth of investigation for a given electrode separation may vary considerably depending on the vertical succession of resistivities in the section. Rather than doing the measurements twice (or more) in two separate passes, we may use a technique such that measurements with several electrode separations are made simultaneously with a single pass along the profile (as it was done for the present fieldwork).

The use of horizontal profiling simultaneously with several different electrode separations is undertaken either to study layers at several different depths, or, more often, to facilitate the distinction between structures that are indistinguishable because they produce overlapping effects at the surface.

Configuration with MN outside

With longer lines, an asymmetrical configuration is sometimes used with two current electrodes and several pairs of potential electrodes exterior to AB and generally adjacent to another: AB MN M'N' ----. There are thus provided a set of configurations with increasing depths of investigation, since these depths are essentially governed by the distance from the potential electrodes to the nearest current electrode.

The measurements for the different pairs of MN may be made simultaneously after which the configuration is moved a distance generally equal to the interval of MN. This

technique permits the use of most of the potential electrodes for measurements at different depths of investigation without actually moving them. The technique also permits one to obtain a large number of readings in a short time.

Presentation of results

In horizontal profiling, with one or more electrode separations, one can, first of all, draw resistivity profiles for a given line on the ground. There will be one curve for each electrode separation used. On the abscissa will be plotted a point representing the position of the midpoint of the configuration at each measurement; at each point the value of the apparent resistivity is plotted on the ordinate using a linear or logarithmic scale as appropriate.

In the case of the asymmetric configuration with MN outside the current electrodes (Figs.7 c, d and e), it is convenient to plot the value of the apparent resistivity at the midpoint between the two potential electrodes. This convention is arbitrary and it is necessary at each time to note on the graph what convention has been used, as well as the position of the current electrodes.

The results of a group of profiles are represented in the form of a map, one for each electrode separation used in the survey. On the map is plotted the midpoint of MN (for symmetrical arrays) or the mid point of B and M for asymmetrical arrays, for each measurement and the corresponding value of the apparent resistivity contours are then drawn representing points of equal resistivity.

The choices of electrode separations as well as the interpretation of the difference in the results given by different electrode separations depend on at least a partial knowledge of the vertical resistivity distribution in the earth. This knowledge usually can be gained only through one or more electrical soundings. Therefore, the execution of these electrical soundings must always precede a study using resistivity profiles (Kunetz, 1966).

3.8.2 Schlumberger array

Advantages:

- less manpower required because only the current electrodes need to be moved at each and every sounding measurement. If at all, the potential electrodes need only be moved occasionally.
- less sensitive to cross-coupling (potential leads shorter)
- less sensitive to lateral inhomogeneties because potential electrodes generally remain fixed. Also if they are moved, lateral effects can be distinguished from layering effects
- better depth of investigation than for the Wenner array
- better resolution between layers with different resistivities
- interpretive aids are generally more developed than for the Wenner array (standard curves, auxiliary graphs, etc.)

Disadvantages:

- more power required as potential electrodes are closer together (small ΔV's). Alternatively more sensitive equipment is required.

3.8.3 Dipole-dipole array

Advantages:

- short AB and MN lines can be used to explore great depths, that is, depth investigation and resolution is better than that of Schlumberger configuration.
- It needs short cables
- fewer problems of current leakage and inductive coupling because of shorter cables

Disadvantages:

- large power required for depth penetration (to produce measurable potential)

- data not so straight forward to interpret
- interpretation procedures and programs are not abundantly available

4. INTERPRETATION PROCEDURES

4.1 Equivalence problem in geophysical interpretation

One of the limitations of the geophysical methods is the non uniqueness of many interpretations. Two types of modeling to be engaged are direct and inverse. In direct modeling one has to develop an equation to describe the effect of the specific physical property variation under study. The equation developed will then tell what effects this variation produces. In most cases, such an equation can be derived and leads to unambiguous results. However, the most often encountered problem is the reverse process of observing effects and then modeling the cause. This is referred to as inverse modeling and typically is more difficult and more ambiguous. For example, many apparent resistivity curves can be due to a variety of subsurface layering configurations. A good geological background and knowledge of the area being studied are essential to arrive at the correct interpretation (Burger, 1992).

It should also be noted that experimentally derived quantities are never exactly determined and experimental error adds a further degree of indeterminacy to that caused by the incompleteness of the field data and the ambiguity associated with the inverse problem. Since a unique solution can not in general be recovered from a set of field measurements, geophysical interpretation is concerned either to determine properties of the subsurface that all possible solutions share, or to introduce assumptions to restrict the number of admissible solutions (Parker, 1977).

4.2 Quantitative interpretation of resistivity soundings when there are more than two horizontal boundaries

The problem of the quantitative interpretation of vertical electrical sounding is to determine the thickness of the different formations having different resistivities from the field sounding curves. The interpretation is based on comparing the field curves with the curves obtained theoretically, or constructed graphically, having suitably chosen parameters. In the case of perfect coincidence of the theoretical with the field curve (complete matching), the values of the field parameters are the same as those of the geoelectical section for which the theoretical or graphical curves have been constructed. It is, however, practically impossible to have an album of theoretical master curves representing all geological situations met in the field. It is thus necessary to devise ways and means of interpreting the observed field curves with the help of a limited number of theoretical curves available in published form.

The analytic graphical auxiliary point method of interpretation (Ebert, 1943; Kalenov, 1957) for the interpretation of two-,three-,four-and multiple-layer curves by using the two layer theoretical master curves and auxiliary point charts has been found quite useful from a practical point of view (Bahattacharya and Patra, 1968).

Resistivity sounding data obtained in the field may appear to represent two, three or even more layers covering the resistive basement rock. Four approaches that may be used in interpreting multiple-layer resistivity sounding data are: -

i) Partial curve matching, in which portions of the field data are matched with the curves computed for a single overburden.

ii) Complete curve matching, using curves computed for mathematical models with two, three or four layers covering an infinite, uniform substratum.

iii) Equivalent curve matching, in which all theoretical curves having similar shapes are grouped to form a single equivalent curve or compares on with field data.

iv) Observation of the positions of maxima and minima on the field data.

In selecting the method of interpretation, three layer sounding field curves are classified according to their shape as,

i) a curve which has a minimum (H- type curve) and indicates the presence of a three layer sequence with the resistivity ratios varying as: $\rho_1 > \rho_2 < \rho_3$

ii) a curve that shows a maximum (K- type curve),with resistively ratios: $\rho_1 < \rho_2 > \rho_3$

iii) a curve that shows a uniform increase in resistivity (A- type curve) with resistivity ratios : $\rho_1 < \rho_2 < \rho_3$

iv) a curve that shows a uniform decrease in resisitivity (Q-type curve), with resistivity ratios: $\rho_1 > \rho_2 > \rho_3$. For more than three layers with different resistivities apparent on the field curve, for example, an HK curve is represented by a sequence of resistivities of the form $\rho_1 > \rho_2 < \rho_3 > \rho_4$.

From the four approaches for the interpretation of multiple-layer resistivity sounding data, the one used in the present work for finding initial model parameters that were fed to the computer for iteration process, is outlined in the section that follows.

4.3 Partial curve matching (using two layer master curve and auxiliary point charts)

Partial curve matching is the procedure most commonly used for preliminary interpretation. Short segments of a resistivity sounding curve are selected for interpretation using the theoretical curves for the single overburden usually starting with the shorter spacing.

As each portion of the curve is interpreted the layers comprising the interpreted portion of the sounding curve are lumped together to form a fictitious uniform layer with lumped resistivity, ρ_e, and a lumped thickness, h_e. This fictitious layer is then used in place of the surface layers when the next portion of the curve is analyzed (Keller and Frischknecht, 1966).

The procedure for matching successive left to right segments of a field sounding curve is as follows:

1) The left hand portion of the field sounding curve, plotted on a transparency of identical log-log scale (62.5 mm), is fitted to as many points as possible on the two layer master curve, maintaining the field axes parallel. This fit provides the location of the first cross or auxiliary point where the field sheet coincides with $\rho_1 = AB/2 = 1$, the origin on the master curve. Hence, ρ_1 and h_1 is read from the coordinates of the field curve that coincides with the master. The best fit segment of the master curve gives $(\rho_2 / \rho_1 = v_1)$ and then ρ_2 can be calculated by $\rho_2 = v_1 \rho_1$. This segment may be extended beyond the fitted portion along the (ρ_2 / ρ_1) line with pencil for a check on the next step.
2) The sounding curve is transferred to the appropriate auxiliary curve set (determined from type-curve of the field curve) where the cross is placed at the origin and the same (ρ_2 / ρ_1) curve of the auxiliary as that in step 1 is drawn with pencil on the sounding curve.
3) Replacing the sounding curve on the two layer master curve and maintaining the (ρ_2 / ρ_1) line from step 2 on the master origin, a second master segment further to the right is fitted to the sounding curve. The second cross is marked over the master origin, giving ρ_{e2}, and h_{e2} where $h_{e2} = h_1 + h_2$ and ρ_{e2} is related to the other parameters by $h_{e2}/\rho_{e2} = (h_1 + h_2)/\rho_{e2}$. At the first cross $\rho_{e1} = \rho_1$ and $h_{e1} = h_1$ and $\rho_3 / \rho_{e2} = v_2$ is obtained from the fitted segment of the master curve and then ρ_3 can be calculated by $\rho_3 = v_2 \rho_{e2}$.

4) The sounding (field) curve is returned to the appropriate auxiliary curve and step 2 is repeated.

5) Repeat step 3 to get ρ_{e3}, h_{e3}, as well as the ratio $\rho_4 / \rho_{e3} = \nu_3$, from the fitted segment of the master curve. Then ρ_4 can be calculated by $\rho_4 = \nu_3 \rho_{e3}$.

6) Repeat steps 4 and 5 until the field curve is completely fitted. The crosses should be marked on the field curve to find the layer thickness h_2, h_3 ...by finding the ratios of $h_2 / h_1 = \mu_1$, $h_2 / h_{e2} = \mu_2$ ... from the corresponding auxiliary charts.

The technique of partial curve matching, although rather crude compared to complete analysis of the sounding curve by computing methods, is quite use full in the field to keep abreast of daily measurements and as a control for the more sophisticated approach later (Telford et al, 1990)

5. DATA COLLECTION, PROCESSING AND RESULT INTERPRETATION

5.1 Data collection

In the present work, two field procedures (vertical electrical sounding and horizontal profiling) discussed in sections 3.7.1 and 3.7.2 respectively were applied along two parallel traverses, which are 1.9 km apart and oriented in the E-W direction. The traverses were chosen close to and in such a way as to pass in proximity to as many functioning piezometer wells as possible, whose water table data were taken during the time of survey for controlling purpose. The topography of the survey area is a flat lying cultivated land. The Schlumberger and the axial dipole-dipole electrode arrays (Figs. 4b and 4c) were used in investigating the vertical and lateral variations of resistivity due to salinity, respectively, of the geologic layers along the two traverses.

Instruments used

The current was supplied to the ground by TSQ-3 low frequency square wave transmitter powered by an 8 horse power Briggs and Stratton motor generator, whereas the potential developed in the ground was measured by IPR-8 receiver. Steel wires of each 1km wound on two reels for the current line and copper wires for the potential line were used along with electrodes.

Vertical electrical sounding (VES)

A total number of ten VES points, five in each traverse, were surveyed. The separations between the VES points are variable, because of the inconvenience encountered due to channels in the farmland for transporting the geophysical equipment. The distances between the VES points along traverse 1 are VES 1-VES 2 = 500 m, VES 2-VES 3 = 500m,

VES 3-VES 4 = 450 m, and VES 4-VES 5 = 1.1km, whereas in the case of traverse 2, VES 6-VES 7 = 850 m, VES 7-VES 8 = 700 m, VES 8-VES 9 = 700 m and VES 9-VES 10 = 450 m apart.

The maximum half current electrode spacing (AB/2) along traverse 1 is 750 m at VES 5 and the minimum is 330 m at VES 1. The intermediate is 500 m at VES 2, VES 3 and VES 4. In the case of traverse 2 the maximum is 500 m at VES 7, VES 8,VES 9 and VES 10 and the minimum is 330 m at VES 6.

Lateral profiling

The axial dipole-dipole with dipole length (a = 5) and n = 1-3 were used for the profiling. The readings for the three slices (corresponding respectively to depths of 5 m, 7.5m and 10 m) were taken with single pass by advancing the potential electrode outside of the current electrodes in steps forward by keeping the current electrodes separation constant, as discussed in section 3.7.2.

Four horizontal profiling lines are conducted, two on each traverse (starting at VES 1 and VES 5 for traverse 1 and at VES 7 and VES 10 for traverse 2) for a maximum length of about 250 m, so as to sample the lateral variation of the electrical resistivity in the area. The total number of data readings taken was 582. The apparent resistivity for each reading of the potential difference (ΔV) in mV and the injected current (I) in mA were calculated by using eqn. (67) and then used to plot the dipole–dipole pseudosections presented in Figures 10, 11, 13 and 14. A plan view showing the locations of the vertical electrical sounding stations and horizontal profiling lines are also shown in Figure 8.

5.2 Data processing

The potential difference measured (ΔV) in millivolts and the amount of current injected in to the ground (I) in milliamperes for the VES surveys were used to calculate the apparent resistivity (ρ_a) in Ohm meters by substituting these values in eqn. (16). The field data were plotted on a double logarithmic paper of 62.5mm cycle length immediately in the field (AB/2 along the abscissa and ρ_a along the ordinate) so as to enable the survey to reduce errors that may be encountered due to improper ground contact of the electrodes, instrument reading errors, errors in electrode lay out, etc.

The set of ρ_a values obtained in the overlapping region with one and the same MN were found to lie on separate curve segments, displaced from each other. These different segments were suitably merged to obtain a single smooth sounding curve. The best way adopted was to shift a segment obtained with a larger MN towards the adjoining previous one obtained with smaller MN. The reason is that ΔV/MN measured for smaller MN values is nearer to the true potential gradient than the value with the larger MN. The predominant contribution to the shifts comes in practice, however, from the differing effect of local inhomogeneities at the old and new positions of M and N electrodes (Parasnis, 1986).

Preliminary interpretations of the smoothed field curves were then performed by the interpretation procedure of partial curve matching technique discussed in section 4.3. The layer parameters from this interpretation were fed to the computer, that use 'RESIST 88' inversion software, as an initial model. This software performs a number of iterations until it obtains theoretical curves that best fit with the observed field curve having least root mean square error. The layer parameters (resistivity and thickness) obtained for each VES point by

this process were then used to construct the geo-electric section and apparent resistivity pseudo-section of the studied area are shown in Figures 9 and 12.

5.3 Result Interpretation

On the basis of the VES data analysis and the available geologic information of the study area (from borehole situated at a distance of about 3.5 km away from traverse two – Figure 8) one can group the subsurface into three main lithologic units:

- thin layer of top dry soil (silty clay loam)
- silty clay
- sand

The lithologic log of the borehole W2 (Appendix B) was thus/therefore used for correlation and to help in the interpretation of results of this geophysical survey.

5.3.1. Geoelectric Section along traverse one

The geoelectric section constructed from the VES data along the first traverse (VES1 to VES5) has a four layered earth structure. The analysis of the geoelectric and pseudosections constructed from the VES observations have provided useful information about the thickness' and depths of geoelectric layers as well as variations in resistivity (Figure 9) in the vertical direction.

Along this traverse the top layer has resistivities in the range of 6.6 - 24.4 Ωm and thickness varying from 1.7 to 1.9 meters . This thin formation is mainly composed of dry silty clay loam. Under this formation it has been noted that a relatively low resistivitylayer (3.2 - 6.4 Ωm) with thickness varying from 7.4 to 9.6 meters is observed. It is interpreted as silty clay which acts as an aquiclude (low hydraulic conductivity).

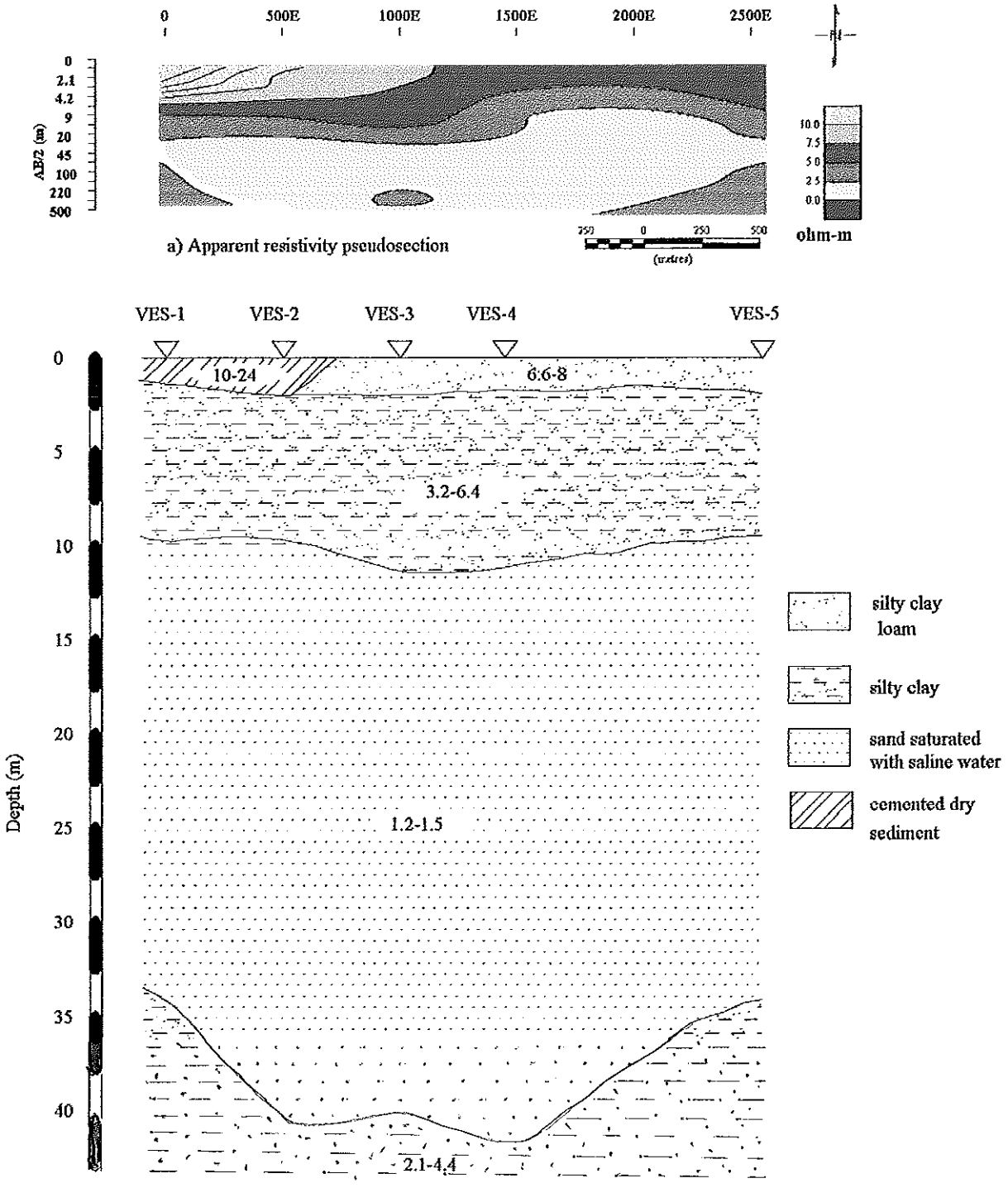

Fig. 9 VES results along traverse 1, Amibara

The third layer has an even low resistivity that is in the range of 1.2 - 1.5 Ωm. This represents sand saturated with saline water and is the probable zone of the semi-confined aquifer system underlying the low permeability layer. The average thickness of this aquifer is 30m and the minimum depth of the saturated zone is 9.2 m around VES 5 and the maximum is 11.4 m around VES 3. But the measurement taken from piezometer AIP 46 at the same position with VES 1 (Figure 8), at the time of survey, indicated a water level at a depth of 4.2 m. This level, 5.2 m above the water saturated zone, may correspond to the potentiometer surface due to partial confinement of the aquifer below it.

The fourth geoelectric layer is again with a relatively higher resistivity value (2.1 -4.4 Ωm) than that of the geoelectric layer just overlying. This is assumed to be as a result of silty clay to some extent moistend by saline water and acts as an aquiclude for the overlying saturated horizon. Relatively speaking, the range of resistivities is less than that of the second geolelectric layer interpreted as silty clay, due to the salinity of the layer above it.

5.3.2 Dipole-dipole pseudosections along traverse one

Profile 1

From the dipole dipole pseudosection (Figure 10) obtained with dipole length a = 5m , n = 1-3 that started at 50 m west of VES 1 and extended to about 175 m east of VES 1, it is possible to see the lateral variation of resistivity along the traverse. The relatively higher resistivity section lies at the top and the low resistivity horizon lies at the bottom, except a sign of upward intrusion nearest to west of VES 1 and at about 60 m east of VES 1 (0 position). This is probably the highly saline water bearing portion of the sand aquifer that is at shallow depth at VES 1.

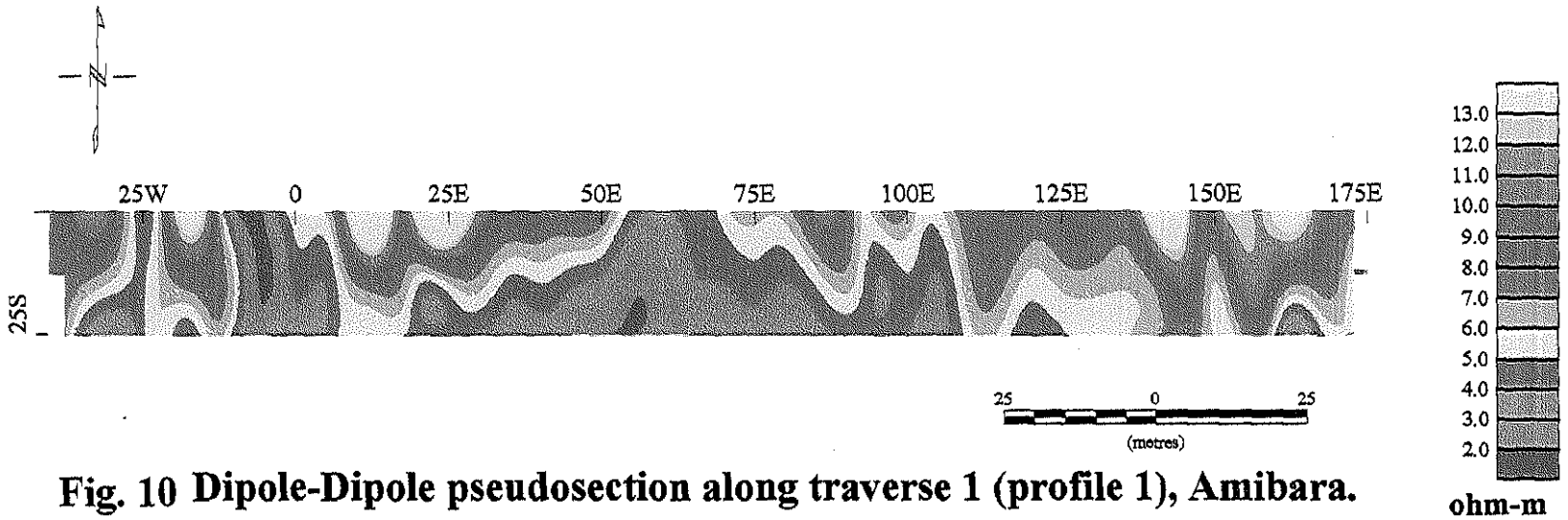

Fig. 10 Dipole-Dipole pseudosection along traverse 1 (profile 1), Amibara.

Dipole lengt : a=5m, n=1-3

Profile 2

The dipole dipole pseudosection contoured from the data taken at the other end of traverse 1 (started at 50 m west of VES 5 for a length of 250 m extending westward) is shown in Figure 11. This indicates similar tendency of relatively resistive section at the top whereas lower resistive section at the bottom. It has also showed that the lower resistivity portion is at shallow depth near VES 5. This manifestation is also clearly observed in the apparent resistivity pseudosection contoured from VES measurements (Figure 9a).

5.3.3 Geoelectric section along traverse two

The Geoelectric section along traverse two was constructed from the final geoelectric parameters of the VES points (VES 6 – VES 10) to describe the vertical and lateral distribution of apparent resistivities over this traverse line (Figure 12b). This section represents a model of three geoelectric layers. The top part of the layer is characterized by a relatively higher apparent resistivity ranging from 4 to 12.6 Ωm with undulating structure and is interpreted as dry silty clay. The thickness of this layer decreases towards VES 10. The maximum thickness is 8.9 m around VES 6 and the minimum is 1 m around VES 10.

The second layer is attributed to the low resistivity zone (1.1-2.2 Ωm). This low resistivity region may be associated with the response of the highly saline fluid content of sand aquifer. This aquifer system starts to branch out in between VES 8 and VES 9 and the flank approaches to the surface to a depth of 1 m near VES 10. This flank is also clearly observed in the apparent resistivity pseudosection (Figure 12a). This will cause the increase of salinaization towards the surface around VES 9 and VES 10 (as an indicator of areas not suitable for plantation at present or the very near future).

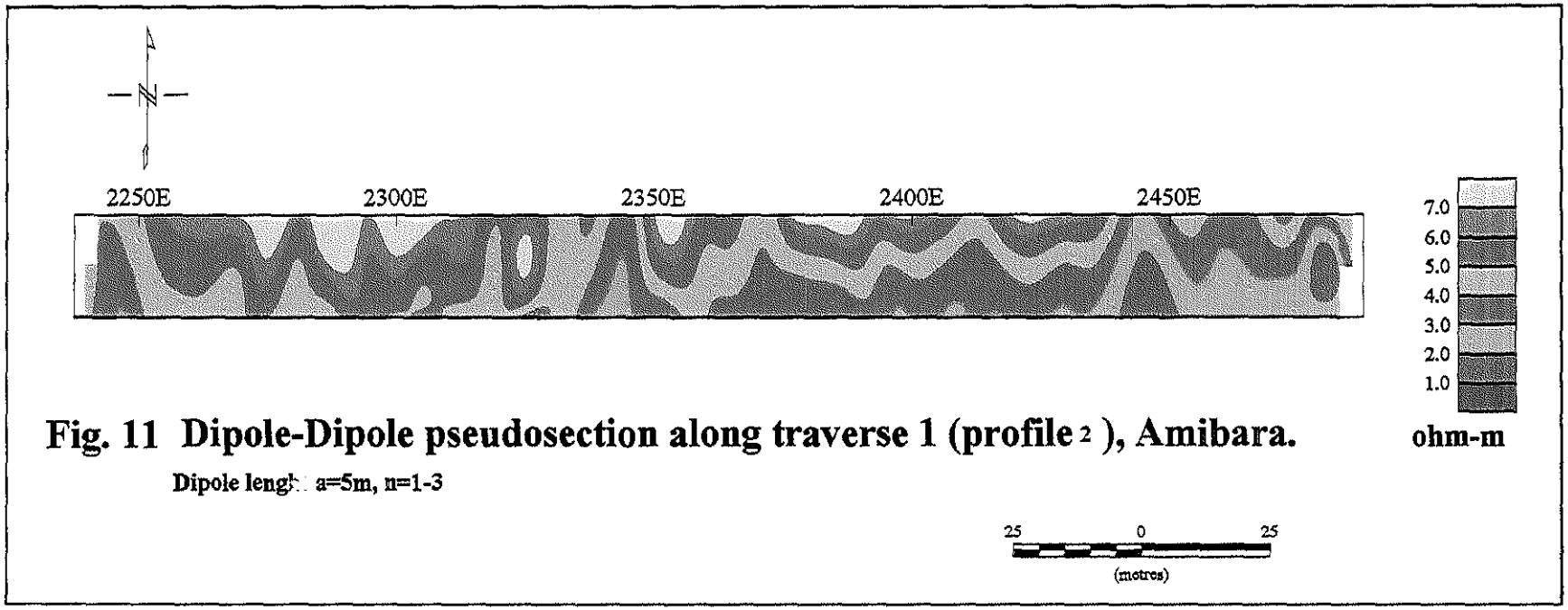

Fig. 11 Dipole-Dipole pseudosection along traverse 1 (profile 2), Amibara.

Dipole lengh: a=5m, n=1-3

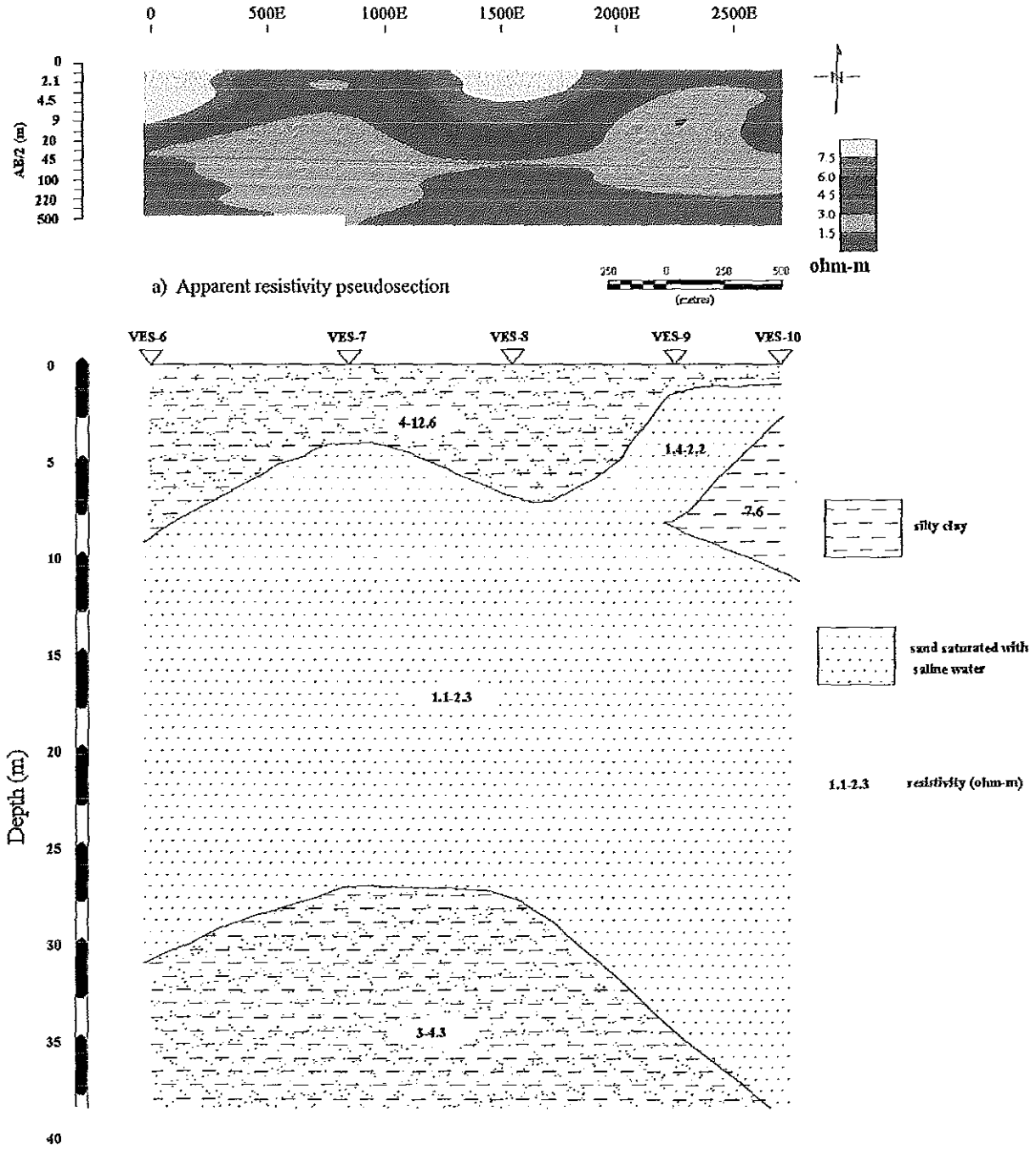

b) Geoelectric section

Fig. 12 VES results along traverse 2, Amibara

5.3.4 Dipole dipole pseudosections along traverse two

Profile 3

The dipole length for this profile is also a = 5 m, n = 1-3. The profiling starts at VES 7 and continues eastwads for a length of about 250 m along the traverse on which VES surveys have been carried out. From the dipole dipole pseudosection (Fig.13), it is clearly observed that the least resistivity zone is dominant west of 900 E while the adjacent formation resistivity to the east is relatively higher except some pockets of low resistivity sections at the bottom. These correspond to the vertical electrical sounding results of Figures 12a and 12b. This means, around VES 7 the least resistive layer is bulged upwards and the adjacent formation is with a relatively higher apparent resistivity. through approximation of the real depth of penetration for the Schlumberger and dipole dipole arrays employed, the apparanet resistivity pseudosection of the sounding survey and the dipole dipole pseudosection of the profiling surveys lie in the same range of depths.

Profile 4

The dipole-dipole pseudosection of profile 4 (Figure 14) was contoured from the apparent resistivity calculated from the current and potential difference readings using eqn. (66) for the same dipole length and number of depth levels as that of profiles 1 – 3.

The profiling starts at 50 m east of VES 10 and continues towards west for a length of 250 m (Figure 10). The low resistivity layer in this section of the survey is at the top between positions 2600E and 2700E except some pockets of relatively higher resistive zones. The low resistivity zone also lies between positions 2550E and extends towards west. This low resistivity zone corresponds to the flank of sand aquifer saturated with saline water near the surface below VES 9 and VES 10 as shown in figures 12a and 12b.

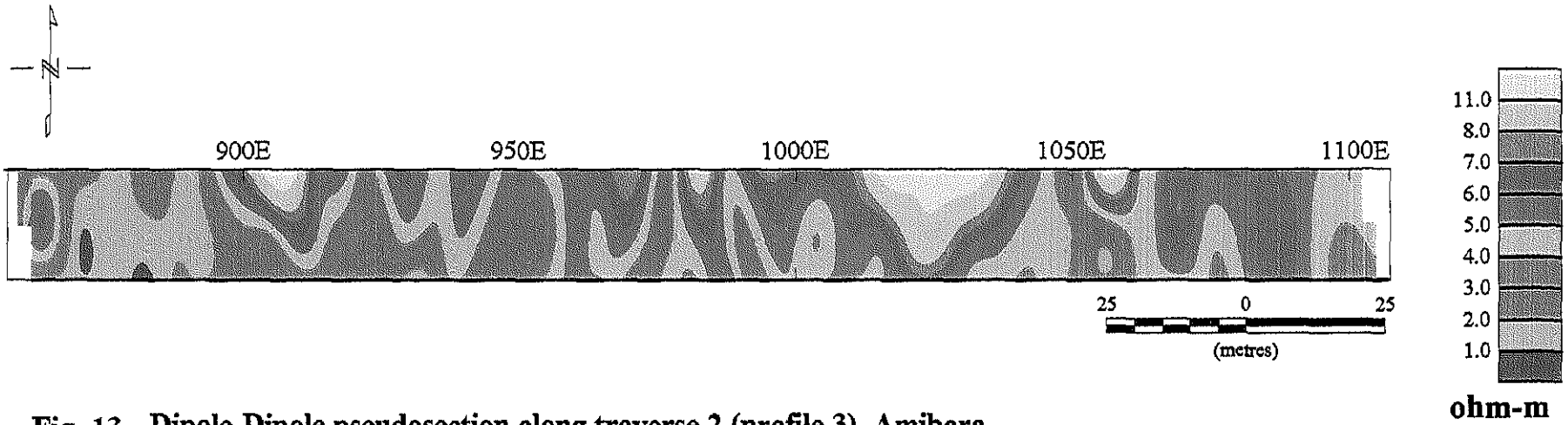

Fig. 13 Dipole-Dipole pseudosection along traverse 2 (profile 3), Amibara.

Dipole length a=5m, n=1-3

Fig. 14 Dipole-dipole pseudosection along traverse 2 (profile 4), Amibara

(dipole length a=5 m, n=1,2,3)

5.4 Conclusions and recommendations

Conclusions

As one of the main objectives of the present work was to delineate the saline and fresh water zones, it was possible to map the probable zone of the shallow aquifer that is saturated with saline water. But due to the thick alluvial deposit in the area, going as deep as beyond 100 meters and problems related to current penetration, it was not possible to map the bedrock and the probable fresh water zone, even with a maximum current electrode separation of AB/2 = 750 m that was used in the present work.

However the work has shown the importance of geophysical methods; especially the electrical resistivity method (vertical electrical sounding and profiling), when applied to map areas of intense salinity that are not favorable for current plantation. The geoelectric sections, for example figure 12b show, which parts of a given farm area (between VES 9 and VES 10 where the saline saturated zone is near the surface) are more affected than the others and which parts could still be used for planting (where the saline saturated zone is at depth).

Recommendations

The electrical resistivity method can conveniently be used in land reclamation projects to follow up of desalinization programs by the drainage system like the one that is currently being carried out in a pilot project at the research center in Amibara.

Geophysical surveys covering different areas of the farm, focusing on sample areas that are subjected to similar type of irrigation and planting conditions, may be employed and the results of such studies may even be used to study the severity of the salinization process. As the process of salinization is a commulative and additive process, whose severity increases by the year the farm is used for planting, the results of such studies would be useful in

planning parts of the farmland which have to be abandoned and desalination program are to be started upon.

In addition, it has been found that after the farms have been abandoned due to salination problems, a process of desalination through the leaching of the salts from the top layers by water percolating from the rains or excess irrigation water that have drained into these abandoned farms, the geophysical methods could effectively be used to delineate these areas which are suitable for re-plantation. Simple profiling surveys extending to a few meters of depth of investigation could be used to identify areas that have been reclaimed through the natural process.

Integrated approach of geophysical surveys, such as

- electrical resistivity method with induced polarization (IP) variation can provide a better picture to study salinity. As the simultaneous decrease of resistivity and IP is a diagnostic feature for locating saline water zones.
- to alleviate the problem of depth of penetration due to conductive layers encountered in this work time domain electromagnetic method (TEM) is recommended.

REFERENCES

Appelo C.A.J, Postma D., 1994. Geochemistry, groundwater and pollution, A.A. Balkema, Rotterdam, pp 296-326

Battacharya P.K and Patra H.P., 1968. Direct current Geoelectric Sounding: Principles and Interpretation. Elsevier Publishing Company,Amsterdam /London/ New York. pp 41-92

Burger H.R, 1992. Exploration Geophysics of the shallow subsurface, Prentice–Hall, Inc. Newjercey.

Callinan B.J. and Webster R.J, 1971. Economic and Social aspects of Saline Water. In: Salinity and Water Use (ed. Talsma T. and Philip J.R.). Macmillan Press, London and Basingstoke. pp 227-242

Chernet T. and GebreEgzabher, Z., 1983. Geothermal geology of the Dofan and Fantale area (Northern Ethiopian Rift, EIGS, Addis Ababa, Note no. 206, pp 1-28

Chernet T., Hart W.K., Aronson J.L. and Walter R.C, (1998). New Age constraints on the timing of volcanism in the Northern Main Ethiopian Rift-Afar Transition Zone. **J. Volcanol. Geotherm. Res.**,Vol. 80, pp 267-280.

Christiansen T.B., Schaefer H.U. and Schonfeld M., 1975. Geology of Southern and Central Afar. In: **Afar Depression of Ethiopia** (ed. Pilger A. and Rosler A.). Schweizerbart, Stuttgart, pp 255-277

Dereje H., Hess M. and Tenalem A., 1996, The Problem of High Rise Groundwater in Amibara Irrigation Project.

Dobrin M.B and Carl H.S, 1988. Introduction to Geophysical Prospecting (4^{th} edition). McGraw-Hill Book Company, New York, pp 1-24

Ebert A., 1943.Grundlagen zur Auswertung geoelektrischer Tiefenmessumgen, Beitr. Angew. **Geophys**, Vol. 10, pp 1-7

Ethiopian Institute of Geological Surveys. Ministry of Mines and Energy (1978). Geological Map of Nazret Sheet (NC 37-15). Scale 1:250,000.

Ethiopian Institute of Geological Surveys. Ministry of Mines and Energy (1981). Geological Map of the Ethiopian Rift Valley. Scale 1:500,000.

Elc- Geotermica Italiana, 1987. Geothermal reconnaissance study of selected sites of the Ethiopian Rift System. Geological Report, Milano, Italy.

FAO, 1983. Additional Geomorphic, Geological and Ground water studies in the Awash Valley. Informal technical report, No. 14

FAO, 1988, Salt-affected Soils and their management, **FAO soil Bulletin**, No.39, pp 1-131

Gasparon M., Innocenti F., Manetti P., Peccerillo A., and Tsegaye A. (1993). Volcanology; petrology and geochemistry of the Pliocene to Recent volcanism in the Debre Zeit area. **African J. Earth Sci.**, Vol. 17, pp 145-165

Ital consult, 1969. Melka Sadi – Amibara proposed irrigation project. Feasibility Study, Geology and Hydogeology, Rome, Part II, Vol. 3,

Kalenov E.N.,1957. Interpretatsia Krivikh Verticalnogo Electrichekogo Zondirovanya, Gostoptekhizdat, Moskva, 470 pp.

Kandiah, A., 1981, Water requirement of some selected crop in the Middle Awash environment, IAR, Addis Ababa, pp 3-23

Kazmin V., Berhe S.M., Nicoletti M., and Petrucciani C., 1980. Evolution of the Northern part of the Ethiopian Rift. In: **Geodynamic Evolution of the Arabian Rift System**. Atti Convegni Lincei. Vol. 47, pp 275-291

Kazmin V., SeifeMichael B., Nicoletti M., and Petrucciani C., 1980. Evolution of the northern part of the Ethiopian rift. Atti. Convegni Lincei, Vol. 47, pp 275-292

Kazmin V., Shifferaw A. and Balcha T., 1978: The Ethiopian basement: stratigraphy and possible manner of evolution. **Geol. Rundschau.** Vol. 67, pp 531-546.

Keller V. and Frischknecht F. C., 1966, Electrical methods in Geophysical Prospecting, Pergaman Pres Inc., pp 90-196.

Koefoed , 0., 1968. The application of the kernel Function in Interpreting Geoelectrical Resistivity Measurements (ed. Kunetz G. and Saxo V.S.) **Geoexploration Nomographs**, Series 1-No. 2

Kunetz G., 1966, Principles of Direct Current Resistivity Prospecting.(ed. Braekken, H. and Van Nostrand, R., 1966). Gebruder Borntraeger, **Geoexploration Nomographs**, Series 1,No1

Meyer W., Pilger A., Rosler A. and Stets J., 1975. Tectonic evolution of the northern part of the Main Ethiopian Rift in Southern Ethiopia. In: **Afar Depression of Ethiopia** (ed. Pilger A. and Rosler A.). Schweizerbart, Stuttgart, pp 362-369

Mohr P.A., 1967. The Ethiopian Rift system. **Bull. Geophys. Obs.**, Addis Ababa, Vol. 11, pp 1- 65

Morbidelli L., Nicoletti M., Petrucciani C. and Piccirillo E.M. 1975. K\Ar ages of the main volcanic events. Main Ethiopian Rift from 8° 10'-9°00' lat. North. In: **Afar Depression of Ethiopia** (ed. Pilger A. and Rosler A., Stuttgart, pp 362-369.

Parasnis D,S., 1986. 4th edition, Principles of Applied Geophysics, J.w. Arrowsmith Ltd., Bristol, pp. 105-170.

Parker R. L., 1977. Understanding inverse theory. **Ann. Rev. Earth planet Sci.**, Vol. 5, pp 35- 64

Peck A.J., 1971. Transport of Salts in Unsaturated and Saturated Soils. In: **Salinity and Water Use** (ed. Talsma T. and Philip J.R.) Macmillan Press, London and Basingstoke. pp 103-123

Roy K..K and Elliott H.M., 1980. Resistivity and IP survey for delineating saline water and fresh water zones, **Geoexploration**, Vol. 18, pp 145-162

Slichter, L. B.,1933. The interpretation of the resistivity prospecting method for horizontal structures. **Physics**, Vol. IV, pp 307-322.

Stefanesco, S. and Schlumberger C., 1930.Sur la distribution electrique Potentielle autour dume prise de terre poncluelle dans un terrain a couhes horizontales homogenes et isotopes. **Journ. De phys. et Radium**,Vol. II, pp 132-140.

Street G.J and Engel R., 1987. The use of Geophysics in defining the causes of dry land salinity in south western Australia, **Expl. Geophysics** Vol. 18, No 1/2

Telford W.M., Gelderat L.P., and Sheriff R., E., 1990. Applied Geophysics, 2nd ed., Cambridge, Cambridge University Press, 770pp

UNDP,1973. Geology, Geochemistry and Hydrogeology of the hot springs of the East African Rift system within Ethiopia. Technical Report, DP/SF/UN/116,United Nations. New York. 285 pp.

Van Nostrand R., and Cook G., and Kenneth L., 1966. Interpretation of resistivity data. **United states Geological Survey professional paper**, Vol. 499, 310pp

Van Overmeeren R.A., 1989. A combination of electrical resistivity, seisnic refraction, and gravity measurements for ground water exploration in Sudan, **Geophysics**, Vol.46, No.9, pp 1304-1313

William Halcrow and Partners, 1982. Amibara Irrigation Project II, Drainage and Salinity Study and Recommendations for Field Drainage (Vol.1), Study and Recommendations,

pp 62-69

William Halcrow and Partners, 1983. Amibara Irrigation Project Water Management Manual.

William Halcrow and Partners, 1985. Master drainage plan for Maika Sadi and Amibora areas final report Vol. 6, Annex B and C.

William Halcrow and Partners, 1986. Master Draimage plan for Melka Sadi and Amibara areas, Main report, Vol. 2

William Halcrow and Partners,1986, Master Draimage plan for Melka Sadi and Amibara areas, Final report Vol. 6, pp 1-3

William Halcrow and Partners, 1975, Angelele-Bolhamo Feasibility study Report, Annex 1-Hydrology

Zanettin B. and Justin-Visentin E. 1974. The volcanic succession in central Ethiopia, the volcanics of the western Afar and Ethioplian Rift margins. Univ. Padova Inst. Geol. Mineral., Mem., 31, pp 1-19

Zanettin B., and Justin-Visentin E., 1975. Tectonical and volcano-logical evolution of the Western Afar margin (Ethiopia)(in: **Afar Depression of Ethiopia**, ed. Pilger A. and Rosler A.), Schweizer bart, Stuttgart, pp 300-309

Zohdy A.A.R., Eaton G.P. and Mabey D.R., (1974). Application of surface geophysics to ground water investigation. Techniques of Water Resources Investigation of United States geological survey, USGPO, Washington.

APPENDIX A and B

Figures A1 to A10 Geoelectric sounding curves at each station.

B Geology of the area from lithologic log and long normal electrical resistivity log

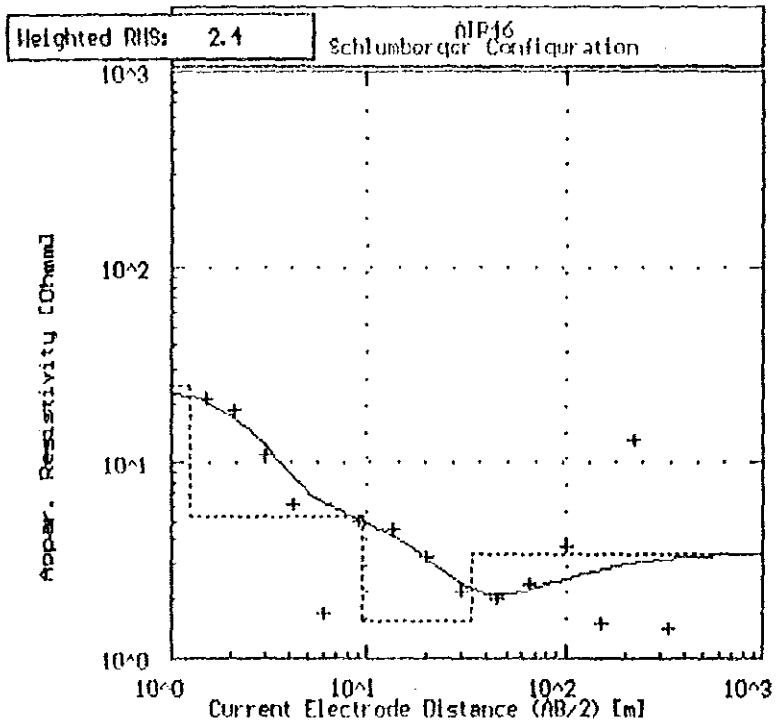

No	Res	Thick	Depth
1	24.4	1.2	1.2
2	5.2	8.3	9.5
3	1.6	24.0	33.6
4	3.4	-.-	-.-

Fig.A1 Geoelectric sounding curve at station VES 1

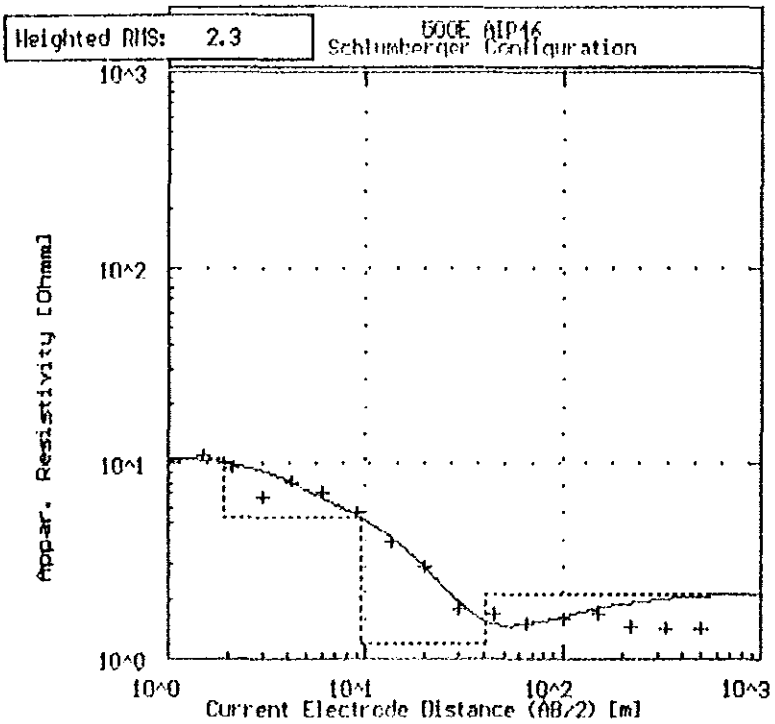

No	Res	Thick	Depth
1	10.7	1.9	1.9
2	5.3	7.5	9.4
3	1.2	30.8	40.2
4	2.1	-.-	-.-

Fig.A2 Geoelectric sounding curve at station VES 2

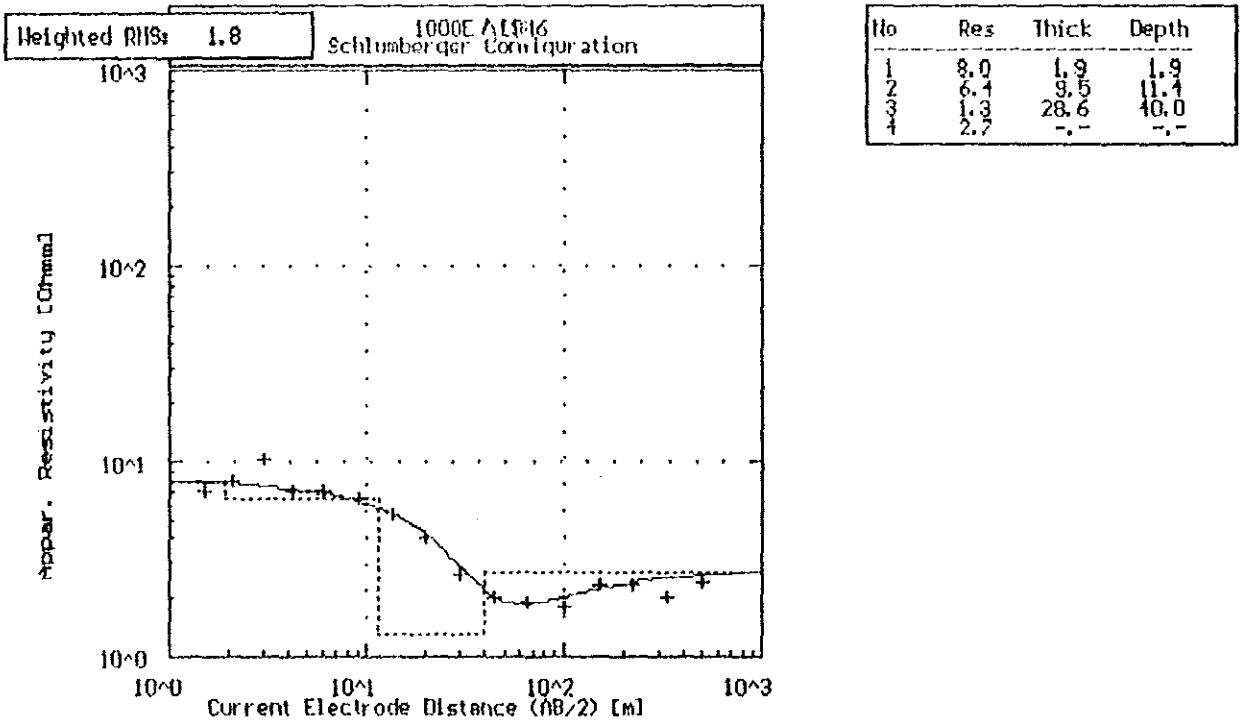

Fig.A3 Geoelectric sounding curve at station VES 3

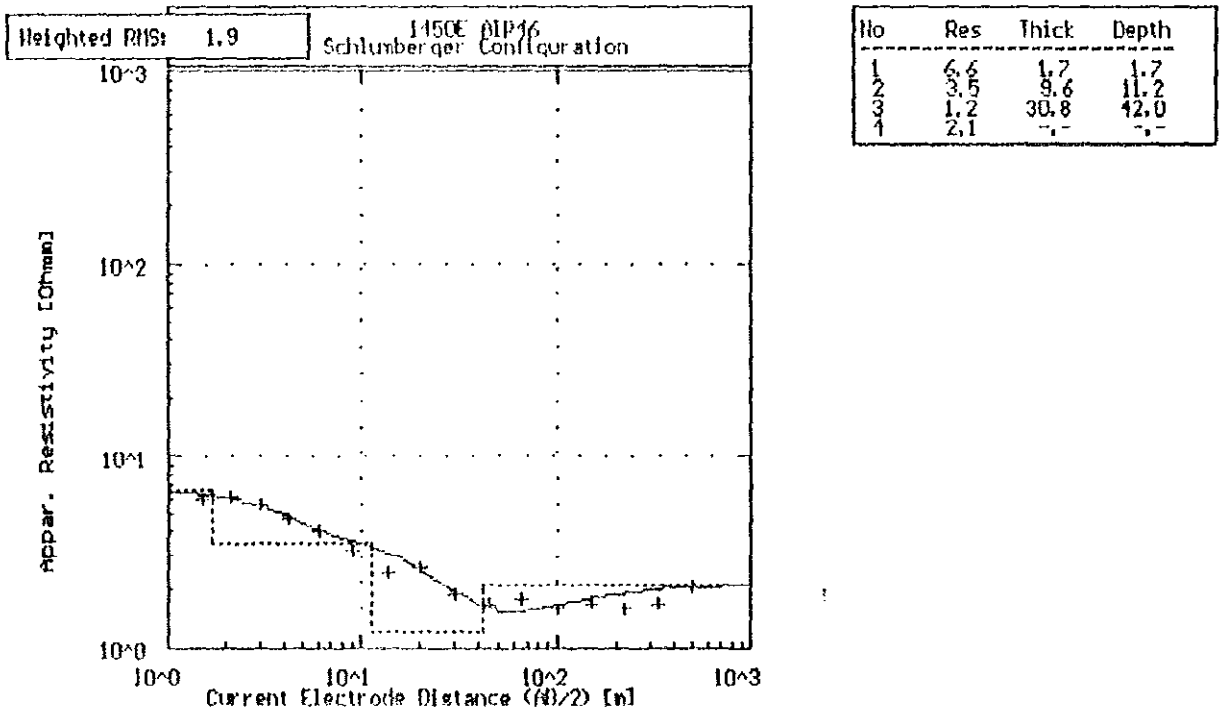

Fig.A4 Geoelectric sounding curve at station VES 4

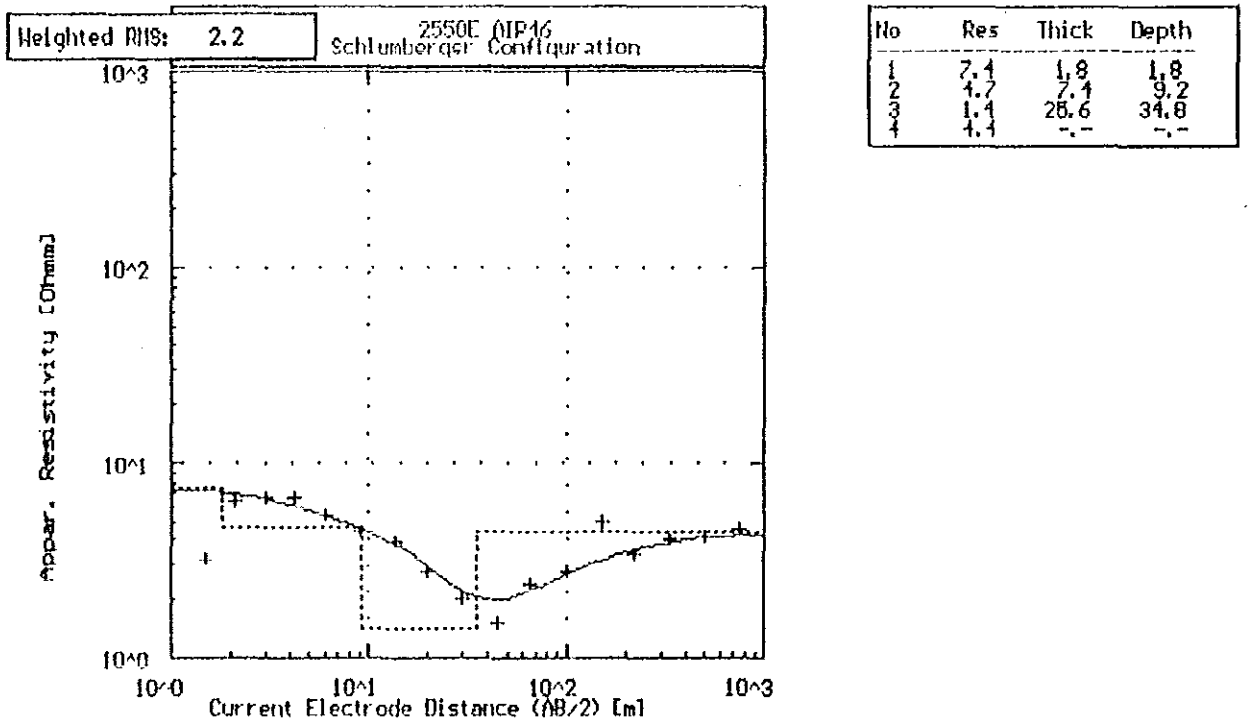

Fig.A5 Geoelectric sounding curve at station VES 5

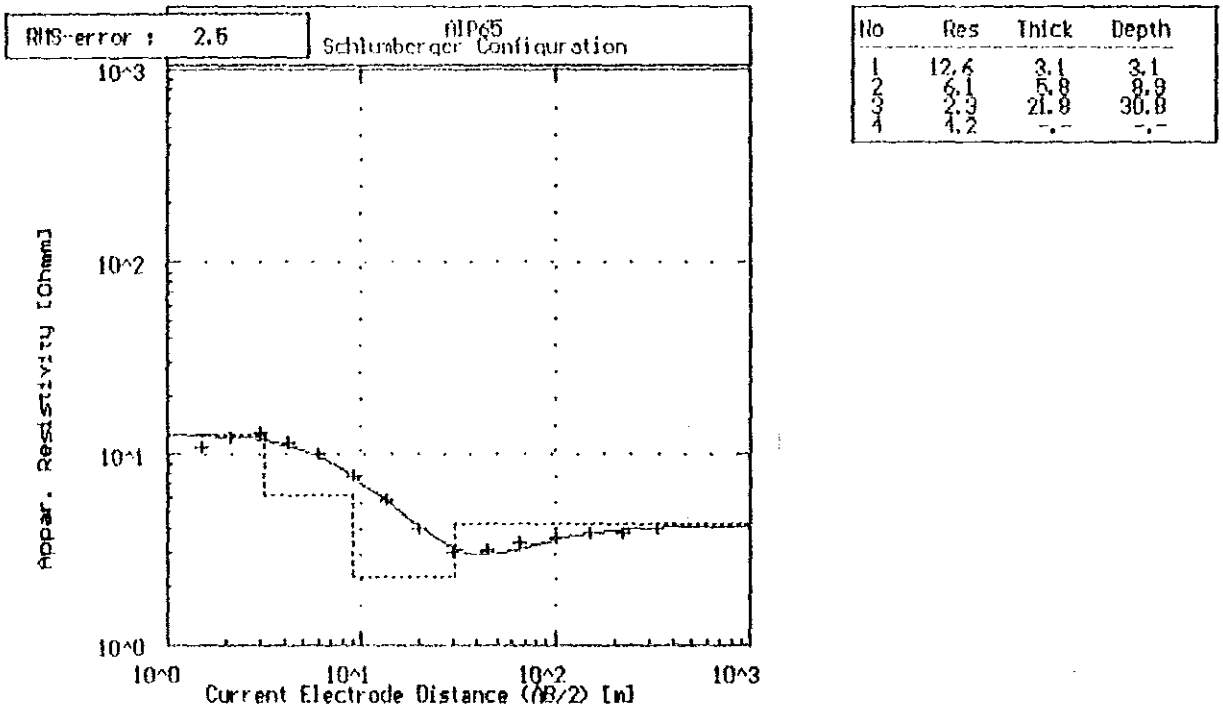

Fig.A6 Geoelectric sounding curve at station VES 6

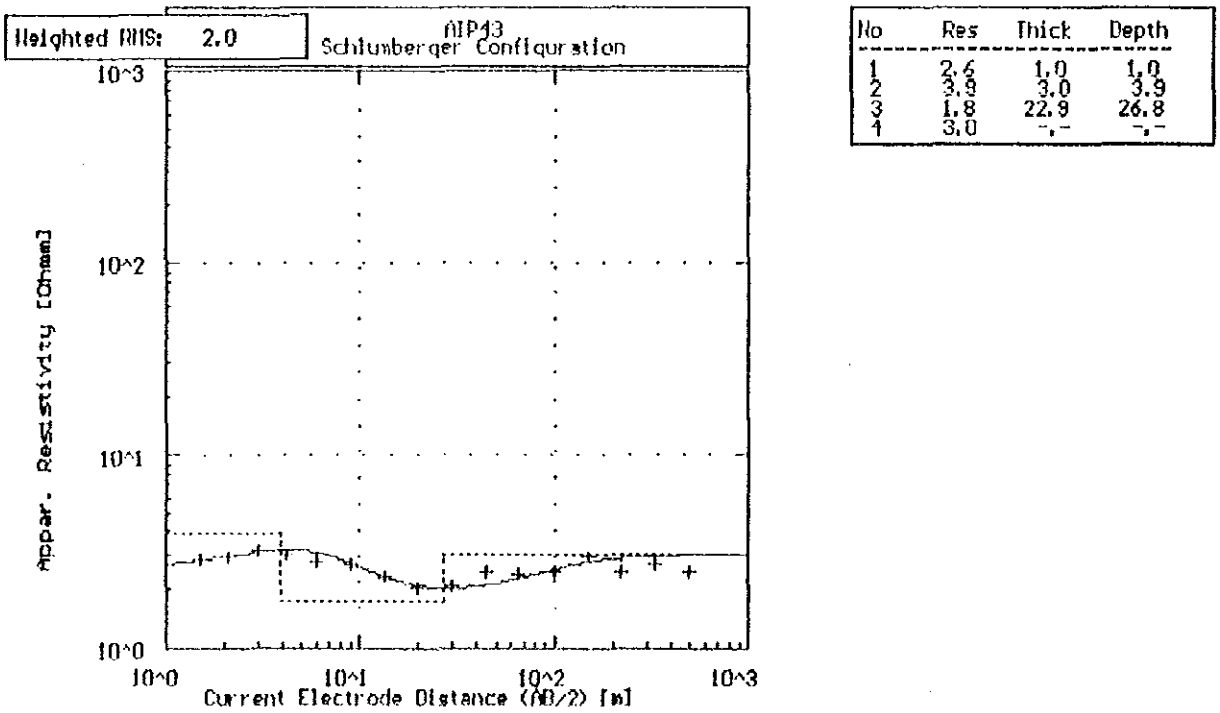

Fig.A7 Geoelectric sounding curve at station VES 7

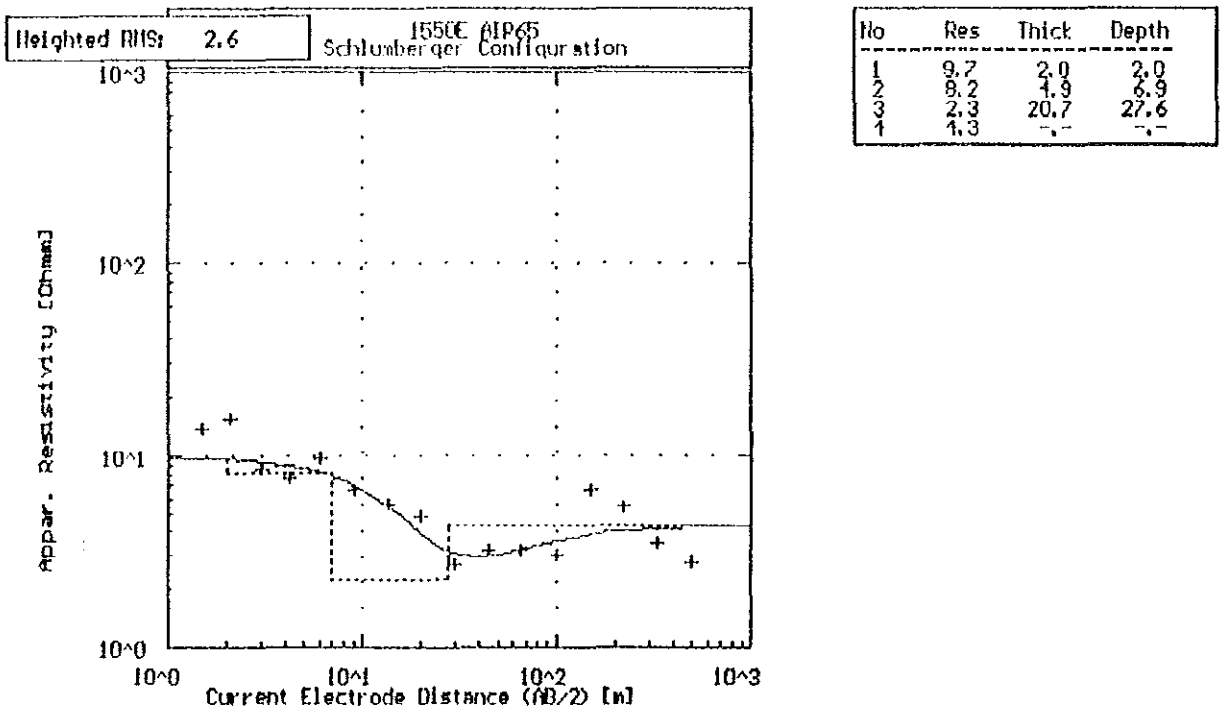

Fig.A8 Geoelectric sounding curve at station VES 8

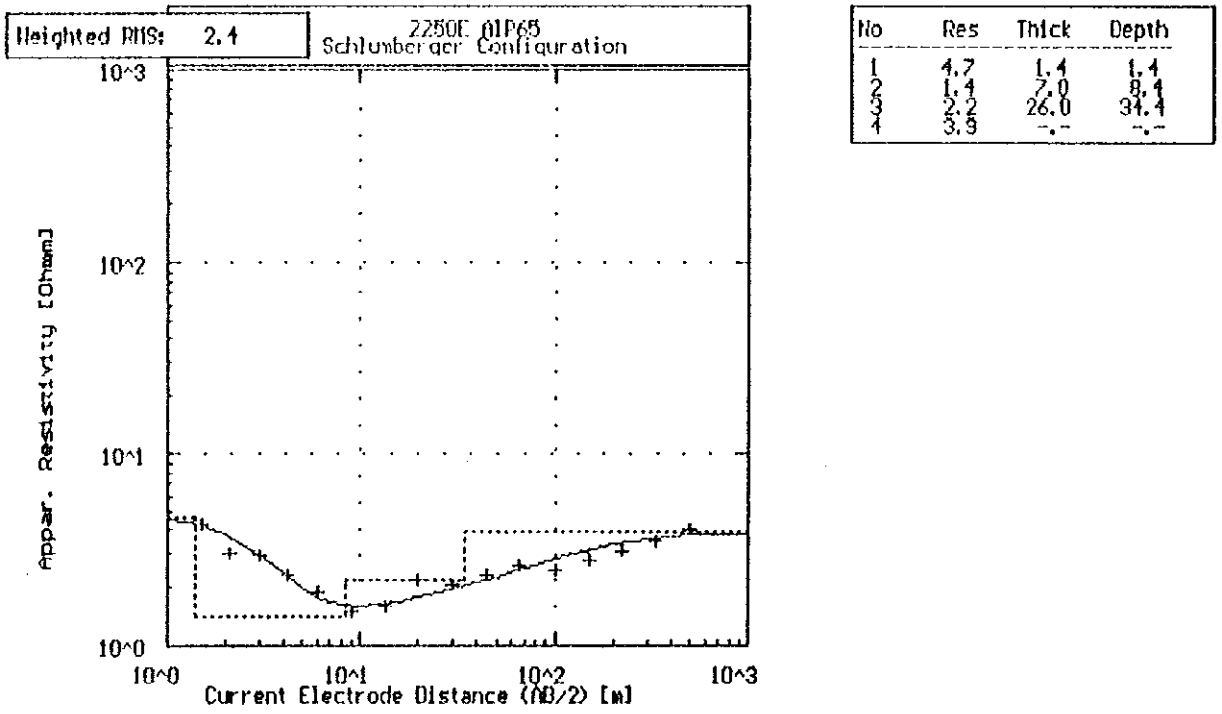

Fig.A9 Geoelectric sounding curve at station VES 9

Appendix B

Geology of the area from the lithologic log and long normal electrical resistivity log.

Well No. 2 (W_2)
Location: At Melka Werer farm, about 3.5 km away from VES-10 (Fig. 8)

Depth (m)	Stratigraphy		Resistivity (Ωm)
	Classification	Description	From long normal electrical resistivity log.
0-9	Clay	-Sanday and silty, grey colour	
9-15	Sand	- Clayey; origin of sand is pumice and pumicious pyro-clastics; grey in color	
15-21	Silt	- very fine; grey in colour	2.6-4.5
21-30	Sand	- very fine to course sand with silt and clay	2.5-7
30-36	Clay	- silty and sandy	6.9-9.5
36-42	Clay+sand	- clay and sand intermixed, black in colour	4.6-7.9
42-57	Clay	- silty and black in colour	3.7-6.3
57-60	Silt	- greyish in colour	5.4—8.4
60-69	- very fine grained and silty	- very fine grained and silty	2.7-9.5 -decreasing downward
69-78	Sand	- course grained sand with sand gravel and clay	2.5-6.3
78-84	Clay	- clay with very few gravel	2.5-4.7

Source: Water Well Drilling Enterprise, 1990 E.C